Testing a one-closure equation turbulence model in neutral boundary layers

Benoît Pinier, Roger Lewandowski, Etienne Mémin, Pranav Chandramouli

Testing a one-closure equation turbulence model in neutral boundary layers

Benoît Pinier*, Roger Lewandowski, Etienne Mémin, and Pranav Chandramouli

IRMAR, UMR CNRS 6625, University of Rennes 1 and FLUMINANCE Team, INRIA Rennes, France

Abstract

We aim to test the performances of an incompressible turbulence Reynolds-Averaged Navier-Stokes one-closure equation model in a boundary layer (NSTKE model). We model a new boundary condition for the turbulent kinetic energy k (TKE), and we achieve the mathematical analysis of the resulting NSTKE model. A series of direct numerical simulation are performed, with flat and non trivial topographies, to obtain by interpolation a generic formula for the Prandtl mixing length $\ell = \ell(Re_\star, z)$, $Re_\star$ being the frictional Reynolds number, and z the distance to the wall. This allows us to carry out numerical simulations at high Reynolds numbers with this turbulence model, in order to discuss its ability to properly reproduce the standard profiles observed in neutral boundary layers, and to assess its advantages, its disadvantages and its limits.

Key words : Fluid mechanics, Turbulence models, Navier-Stokes Equations, Direct numerical simulations, Boundary layer, Channel flows.

2010 MSC: 76D10, 76F40, 35Q30.

Contents

*Corresponding author: benoit.pinier@univ-rennes1.fr

1 Introduction

The simulation of a turbulent flow by a direct numerical simulation (DNS) using the Navier-Stokes Equations (NSE) remains today – and likely for a very long time – out of reach for a high Reynolds number Re. Indeed, the Kolmogorov's laws imply that $O(Re^{9/4})$ degrees of freedom are necessary to do so, which is too large in term of computing power for realistic turbulent flows, such as geophysical flows, the Reynolds number of which is larger than 10^8. This is why turbulence models are inescapable. Among all turbulence models, two main classes can be distinguished: the Large Eddy Simulation models (LES), such as Smagorinsky's model, and the Reynolds-Averaged Navier-Stokes (RANS) models, such as the $k-\varepsilon$ model (see Chacon-Lewandowski [15] , Schlichting-Gersten[35] , Pope [42] and Sagaut [44]).
This paper combines modeling, mathematical analysis and numerical simulations. The aim is to investigate the ability a basic incompressible RANS model to faithfully reproduce a neutral boundary layer based on series of numerical simulations, after having modeled suitable boundary conditions and carried out the mathematical analysis of the resulting PDE system. The starting point is a by-product of the $k-\varepsilon$ model with only one closure equation, specified by the following equations (Chacon-Lewandowski [15] chapter 6,

Wilcox [51]). :

$$
(1.1)\quad \begin{cases} (\overline{\mathbf{v}}\cdot\nabla)\,\overline{\mathbf{v}} - \nabla\cdot\left[(2\nu + C_v\ell\sqrt{k})\,D\overline{\mathbf{v}}\right] + \nabla\overline{p} = \mathbf{f}, & (i)\\ \nabla\cdot\overline{\mathbf{v}} = 0, & (ii)\\ \overline{\mathbf{v}}\cdot\nabla k - \nabla\cdot((\mu + C_k\ell\sqrt{k})\nabla k) = C_k\ell\sqrt{k}|D\overline{\mathbf{v}}|^2 - \ell^{-1}k\sqrt{|k|}, & (iii) \end{cases}
$$

where "$\nabla\cdot$" is the divergence operator and

i) $\overline{\mathbf{v}} = (\overline{u}, \overline{v}, \overline{w})$ is the long time average of the flow as considered in Berselli-Lewandowski [7] and Lewandowski [31] (or any stationary statistical mean, which does not make any difference thanks to the ergodic assumption about turbulent flows, see for instance in Frisch [22]), $\overline{p}$ the mean pressure, k the turbulent kinetic energy (TKE), $D\overline{\mathbf{v}} = (1/2)(\nabla\overline{\mathbf{v}} + \nabla\overline{\mathbf{v}}^T)$ the deformation tensor,

ii) $\nu > 0$ is the kinematic viscosity of the flow, $\mu > 0$ a diffusion coefficient, $\mathbf{f}$ a source term expressing possible external forces,

iii) In system (1.1), the functions

$$
(1.2)\qquad \nu_t = \nu_t(k) = C_v\ell\sqrt{k}, \quad \mu_t = \mu_t(k) = C_k\ell\sqrt{k},
$$

are the eddy viscosity and the eddy diffusion, ℓ is the Prandtl mixing length, $C_v > 0$ and $C_k > 0$ are dimensionless constants. These eddy functions ν_t and μ_t may be truncated for large values of k for reasons related to mathematical analysis, which will be discussed in the rest of this article.

iv) the term $C_k\ell\sqrt{k}|D\overline{\mathbf{v}}|^2$ in the equation (1.1, (iii)) is the dissipation of the mean flow, generating turbulent kinetic energy, whereas $\varepsilon = \ell^{-1}k\sqrt{|k|}$ is the mean dissipation of the fluctuations, damping the TKE.

This type of one-closure equation model can be a good alternative to the full two-closure equations $k-\varepsilon$ model, which is expensive and very hard to implement numerically, although very accurate and effective. Evolutionary versions of (1.1) have been used for large scale oceanic simulations (See Blanke-Delecluse [8], Lewandowski [29]), and also in marine engineering to simulate a 2D flow around a fishing net, which has been studied by Lewandowski-Pichot [33].
The model is known as the Prandtl one-equation model (see in Wilcox [51]). Others one equation closures exist in literature such as the Baldwin-Barth model [4], Spalart-Allmaras model [47]. All such models generate correct results for a flat plane bounded flow. An extensive review of RANS model is available in the publication of Argyropoulos and Markatos [2]. The mathematical foundation of the models are available in Wilcox's book [51]. Recently Fares and Schröder [20] developed another one equation models derived from the $k-\omega$ two equations model with good performance.

To fix ideas, let us consider a 3D flow over a plate, placed at $z = 0$. The flow domain is the half space $\{z \geq 0\}$, divided in two regions:

i) the boundary layer $\{0 \leq z \leq z_0\}$, z_0 being the height of the boundary layer,

ii) $\{z_0 \leq z\}$, which is the computational domain and where a turbulent model is implemented.

This raises the questions of the boundary conditions, in particular at the bottom of the computational domain $z = z_0$. In this place, the boundary condition satisfied by the mean velocity is usually a wall law, one of the most popular being the Glaucker-Manning law (see in Chacon-Lewandowski [15, Chapter 5])[1]:

$$\overline{\mathbf{v}} \cdot \mathbf{n} = 0, \quad -[(2\nu + \nu_t) D\overline{\mathbf{v}} \cdot \mathbf{n}]_\tau = \alpha_v |\overline{\mathbf{v}}| \overline{\mathbf{v}}, \quad \text{at } z = z_0. \tag{1.3}$$

A more general set of wall functions can be found in Kalitzin et al [24].
When the friction Reynolds number is small, the Dirichlet boundary condition can be applied for the velocity (Wilcox [51] Parente-Gorlé [38]).
The natural boundary condition for the TKE is,

$$k = |\overline{\mathbf{v}}|^2 \quad \text{at } z = z_0, \tag{1.4}$$

which connects in a non linear way the TKE to the velocity at the bottom of the computational domain.
All this, equations and boundary conditions, yields a turbulence model. If the main question is to assess the ability of such a model to simulate turbulent flow from a practical point of view, we must begin to question its mathematical structure, which leads to purely theoretical considerations.

Mathematical motivation and new boundary condition. We know that the resulting boundary value problem given by the system (1.1) and the boundary conditions (1.3) (wall law for $\overline{\mathbf{v}}$) and (1.4) (boundary condition that links $\overline{\mathbf{v}}$ and k), for a given smooth function $\ell = \ell(\mathbf{x})$, yields serious mathematical and numerical complications mainly because of the relation (1.4) between $\overline{\mathbf{v}}$ and k at the bottom. In particular, we have never been able to demonstrate the existence of a solution to this problem in the evolutionary case, and although we have a proof in the steady-state case as considered here (see in in Chacon-Lewandowski[15]), the proof is particularly technical and long, which is not satisfactory. This is the reason why we looked for an alternative condition to (1.4), which decorrelates the velocity of the TKE, while preserving the physical characteristics of the flow and leading to a better treatment from the point of view of mathematical analysis.
It is important to note that this mathematical analysis that we undertake in this paper, namely the theoretical question of the existence of solutions to the system of partial differential equations used to simulate the flow, has a considerable impact on the question of stability and consistency of the numerical schemes used for the numerical simulations, which amounts to a theoretical validation of these simulations, regardless of DNS results and/or any in situ data, which unfortunately we do not have here.
By adapting the reasonings which allow the obtaining of the wall law for the velocity such as (1.3), we get in this paper the following nonlinear law for the TKE at the bottom of the numerical domain:

$$\mu_t(k) \frac{\partial k}{\partial n} = \alpha_k k \sqrt{k}, \quad \text{at } z = z_0, \tag{1.5}$$

where $\mu_t(k)$ is the eddy viscosity diffusion, such as given by equation (1.2), α_k a dimensionless coefficient that we have calibrated according to the DNS. Considering this boundary condition instead of (1.4), we get a more affordable mathematical structure than that provided by the relation (1.4) between k and $\overline{\mathbf{v}}$. In particular, we are able to prove in this paper, by a proof not too complicated, the existence of a weak solution to the system of

[1] Let $\mathbf{n}$ denotes the outward normal vector at the boundary, and for a given vector $\mathbf{w}$, $\mathbf{w}_\tau = \mathbf{w} - (\mathbf{w} \cdot \mathbf{n})\mathbf{n}$ its tangential part. We refer to ν_t as any eddy viscosity.

equations (1.1), with the boundary conditions (1.3) (wall law for the velocity) and (1.5) (new boundary condition for the TKE). This is the Theorem 3.1 below, the proof of which is developped in Section 3, which is the main theoretical result of this paper.

Remark 1.1. *The resulting model, given by the equations* (1.1), (1.3) *and* (1.5), *is appointed by the acronym NSTKE.*

Remark 1.2. *Homogenenous Neumann boundary condition may also be prescribed for the TKE at* $z = z_0$, *that is*

$$\frac{\partial k}{\partial n} = 0,$$

see in Cindori-Juretié *[17],* Liu *[34], which comes within the scope of our theoretial study, in a simplified way.*

Numerical framework and mixing length. Once the structure of the new model is understood, the next step is to evaluate its numerical performances inside a boundary layer, which means taking z_0 at least of order of the height of the viscous sublayer. We will do so in the case of a flat bottom, which is the simple case with which to start, then in the case of a non trivial topography as displayed in figure 1, called the rough case. The aim is to test topology that are small compared to the turbulent boundary layer height such as grass, sand (or wave for oceanic boundary layer). Problems related to buildings or hills are not treated in this paper.

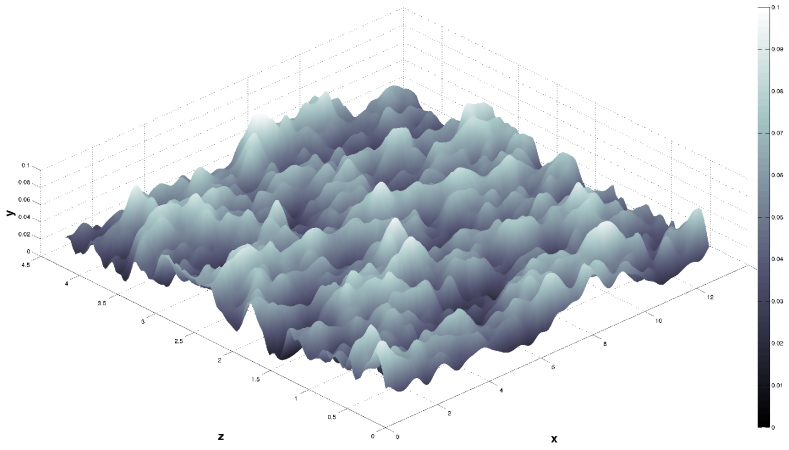

Figure 1: Non trivial topography, also called the rough case.

Another motivation is that the model is easy to implement. The mixing length ℓ is computed by the product of two functions that depend only on the distance, determined by DNS and an extrapolation method, which yields the need to determine four dimensionless coefficients, that we assume to only depend on the friction Reynolds number. For comparison, Spalart-Allmaras [47] model is closed with eight closure coefficients and three damping functions. Baldwin-Barth model seven closure coefficients and three damping functions, Wilcox [51]. Furthermore, the proposed model is universal. The implementation of the wall function is also easy in solvers like OpenFoam.

It is important here to explain how the mixing length ℓ is determined, which is one of the main contributions of this study. In the full $k-\varepsilon$ model, it is deduced from k and ε by the standard formula

$$\ell = \frac{k^{3/2}}{\varepsilon}, \tag{1.6}$$

From DNS data of small and high Reynolds turbulent channel flow, k and ε are obtained assuming that k, ε and ℓ are homogeneous in the $x-y$ axes, we evaluate $\ell = \ell(z, Re_\star)$ at the grid points, properly averaging the data raised from the DNS. We then interpolate the collected sets of numerical values to get a general formula in both flat and rough cases (see formula (4.17) and (4.18), complemented by (4.19), (4.21) and (4.22) for the calculation of the different dimensionless coefficients)[2]. Our DNS are compared to the DNS of Moser et al. [27, 37], which serves as the benchmark for our results.
To return to performance, comparing to other models, note that eddy viscosity computed by both Spalart-Allmaras and Baldwin-Barth models do not decay at the end of the turbulent boundary layer (see in Wilcox [51]). In our model, given the expression for the turbulent mixing length, the computed TKE and the turbulent mixing length decrease (and remain positive) at the edge of the boundary layer leading to a decaying eddy viscosity. This fundamental property avoid the extra dissipation at the summit of the boundary layer as seen in algebraic models (0 equation closure) Smith-Cebeci [46] and Baldwin-Lomax models [5].

Numerical results. With numerical formula (4.17) and (4.18) for ℓ, several numerical simulations with the NSTKE model have been performed up to $Re_\star = 10000$, in both flat and rough cases, after having evaluated the roughness coefficients contained in the boundary conditions. There is no universal turbulence model, and this one is neither better nor worse than another. However, compared to others, the existence of weak solutions provides us some guarantees. Note also that the numerical simulation is as important as the model itself, and consistency analysis of the scheme used should be also performed. This an open problem left for future studies. In this work only a numerical assessment of the convergence has been performed.
The NSTKE model behaves properly in the flat case, which validates our approach. However, the results are less good in the rough case. This does not mean that the model and our approach have reached their limits, and the present study opens several questions. We clearly do not have enough DNS in the rough case for the determination of ℓ. Moreover, in this case, the assumption $\ell = \ell(z, Re_\star)$ must be called into question, in favour of $\ell = \ell(x, y, z, Re_\star)$. Last but not least, this first series of results shows that the topography should be strongly taken into account in the calculation of the roughness coefficients, and it remains an open question to know how to find a universal and simple way for doing this, which is one of the main challenge in the field (see the "bulk algorithm" in Pelletier [40] for instance).

Organization. This paper is is organized as follows. We carry out in Section 2 the modeling of the new TKE boundary condition (1.5), based on a standard assumption about the eddy viscosity in the subviscous layer and a Taylor expansion, following the usual outline for deriving wall laws.
We prove in Section 3 an existence result to the resulting NSTKE system. We briefly review the state of the art about NSTKE systems. Then we carefully set the functional spaces and the norm we use (see Lemma **??**), that alllows us to define the notion of weak

[2] In the process, we also calculate the values of the constants C_v and C_k involved in the eddy viscosities

solutions for this system (see (3.63), (3.64), (3.65) below), following the same pattern as in Chapter 7 in Chacon-Lewandowski [15], One of the main characteristics of the problem is the equation for k which is an elliptic equation with a right hand side (r.h.s) in L^1 whose boundary condition is a non linear Neumann Boundary condition. Such elliptic equations with r.h.s in L^1 and nonlinear Neuman BC have not been consider before so far we know. This is why we prove in Lemma 3.2 below an estimate *à la* Boccardo-Gallouët [10] for such equations, which is the main novelty in this analysis part.
Section 4 is devoted to display several DNS, that yields to numerical formula for the Prandtl mixingh length ℓ (see (4.17) and (4.18) below), as well as the setting of the constants.
We show in Section 5 the results of the simulations from the NSTKE model, using the recursive algorithm given in subsection 5.1, both in the flat and in the rough cases. We also carry out a numerical convergence analysis of the algorithm.

2 Boundary condition modeling

The aim of this section is the derivation of the new boundary condition (1.5) for the turbulent kinetic energy, denoted by the acronym TKE, that is

$$-\mu_t \frac{\partial k}{\partial \mathbf{n}} = \alpha_k k\sqrt{k} \quad \text{at } z = z_0 \tag{2.1}$$

Before doing this, we need to set up carefully the geometrical framework. Then we recall the classical log law of the boundary layer mean velocity profile.

2.1 Geometry and boundary layers assumptions

The computational box Ω is defined by (see figure 2)

$$\Omega = [0, L_x] \times [0, L_y] \times [0, L_z].$$

For simplicity, we assume that the flow field $(\overline{\mathbf{v}}, \overline{p}, k)$ satisfies periodic boundary conditions in the x and y directions. To be more specific, $(\overline{\mathbf{v}}, \overline{p}, k)$ is defined on $\mathbb{R}^2 \times [0, L_z]$, and when it is at least of class C^2, for $\psi = \overline{\mathbf{v}}, \overline{p}, k$,

$$\forall\, (m,n) \in \mathbb{N}^2, \quad \forall\, (x,y,z) \in \Omega, \quad \psi(x + nL_x, y + mL_y, z) = \psi(x,y,z). \tag{2.2}$$

To carry out the modeling process, we assume that in the boundary layer, the mean velocity $\overline{\mathbf{v}}$ has a constant direction, $\overline{\mathbf{v}} = (\overline{u}, 0, 0)$, and is homogeneous in the x-y axes. Therefore, $\overline{u} = \overline{u}(z)$, which is a standard assumption.
It is generally accepted (Chacon-Lewandowski [15], Lewandowski [29], Mohammadi-Pironneau [35], Pope [42]) that there exists $0 < z_0 << z_1$ such that in the absence of stratification or buoyancy effects, $\overline{u}$ has in $[0, z_1]$ the following profile,

$$\forall\, z \in [0, z_0], \qquad \overline{u}(z) = \frac{u_\star}{\kappa} \frac{z}{z_0}, \tag{2.3}$$

$$\forall\, z \in [z_0, z_1], \qquad \overline{u}(z) = \frac{u_\star}{\kappa} \left(\log\left(\frac{z}{z_0}\right) + 1 \right), \tag{2.4}$$

where $u_\star$ denotes the friction velocity, given by

$$u_\star = \sqrt{\nu \frac{\partial \overline{u}}{\partial z}(0)}, \tag{2.5}$$

and κ is the Van Karmàn constant, the numerical value of which is estimated between 0.35 and 0.42 (Foken [21]). Here z_1 denotes the height of the boundary layer.

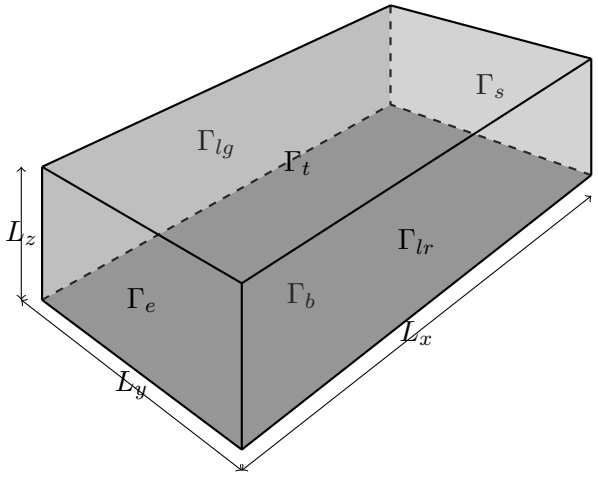

Figure 2: 3D Representation of Ω

2.2 Boundary condition for the TKE

We model in this section a boundary condition for the TKE at $z = z_0$, alternative to (1.4). In order to proceed, we first must:

i) Determine the eddy diffusion coefficient μ_t in $[0, z_0]$,

ii) Settle the profile of the TKE k in the same region, in which we assume $k = k(z)$.

i) According to standard use, we assume that in $[0, z_0]$, the flow is driven by the mixing length ℓ and the friction velocity $u_\star$, and that

$$\ell = \kappa z.$$

Therefore, as z and $u_\star$ are dimensionally independent, $(z, u_\star)$ is a dimensional basis (see Chacon-Lewandowski [15, Chapter 3]). We deduce from straightforward calculation based on dimensional analysis the usual formula:

$$\forall\, z \in [0, z_0], \quad \mu_t(z) = \kappa_\mu u_\star z, \tag{2.6}$$

where κ_μ is a dimensionless constant.
ii) It is natural to set $k(0) = 0$ and $k(z_0) = \overline{u}^2(z_0)$, which yields, by (2.3),

$$k(0) = 0, \quad k(z_0) = \frac{u_\star^2}{\kappa^2}. \tag{2.7}$$

Following (2.3) we enforce k to be linear in the viscous sublayer[3], which leads by (2.7) to

$$\forall\, z \in [0, z_0], \quad k(z) = \frac{u_\star^2}{\kappa^2}\frac{z}{z_0}. \tag{2.8}$$

We derive from these modeling hypotheses, the following result.

Proposition 2.1. *Assume that (2.8) and (2.6) hold. Then the following expansion holds:*

$$\forall\, z \in]0, z_0], \quad \mu_t \frac{dk}{dz} = \kappa\kappa_\mu \left(\frac{z_0}{z}\right)^{\frac{1}{2}} k\sqrt{k} + o(z). \tag{2.9}$$

[3]Notice that, even though it seems reasonable, this is an arbitrary choice, and that another choice would yield another boundary condition.

Proof. We expand $k(z)$ between 0 and z:

$$k(0) = k(z) - z\frac{dk}{dz}(z) + o(z). \tag{2.10}$$

By (2.8), we get

$$z\frac{dk}{dz}(z) = \frac{u_\star^2}{\kappa^2}\left(\frac{z}{z_0}\right) + o(z). \tag{2.11}$$

We combine (2.6) and (2.11), and we get

$$\mu_t\frac{dk}{dz}(z) = \frac{\kappa_\mu}{\kappa^2}u_\star^3\left(\frac{z}{z_0}\right) + o(z). \tag{2.12}$$

The relation (2.8) can be rewritten for $z > 0$ as

$$u_\star = \kappa\left(\frac{z_0}{z}\right)^{\frac{1}{2}}\sqrt{k(z)},$$

that we insert in (2.12) to eliminate $u_\star$, which yields (2.9). □

When we neglect the remaining term in (2.9), we get at $\Gamma_{b,c} = \{z = z_0\}$ the following boundary condition for k:

$$\mu_t\frac{dk}{dz} = \alpha_k k\sqrt{k}, \tag{2.13}$$

where $\alpha_k = \kappa\kappa_\mu$. By symmetry, a similar analysis can be carried out at the top of the computational box. Therefore, we can summarize the results in the following general setting:

$$-\mu_t\frac{\partial k}{\partial \mathbf{n}} = \alpha_k k\sqrt{k} \quad \text{at} \quad \mathbb{R}^2 \times (\{z = z_0\} \cup \{z = L_z - z_0\}) = G_c. \tag{2.14}$$

Remark 2.1. *Note that according to formula (1.6), the boundary condition (2.14) can be rewritten as*

$$-\mu_t\frac{\partial k}{\partial \mathbf{n}} = \alpha_k \ell\varepsilon. \tag{2.15}$$

This is as if at the computational boundary G_c, we decided that the TKE is damped by the mean dissipation of the fluctuation scaled by the mixing length, which is in coherence with the TKE equation and some way of a physical interpretation.

2.3 Synthesis of equations

This subsection aims to summerize the geometry, the equations and the boundary conditions. Let Om_c denotes the infinite strip

$$\mathrm{Om}_c = \mathbb{R}^2 \times [z_0, L_z - z_0], \tag{2.16}$$

and G_c its top and bottom

$$G_c = \mathbb{R}^2 \times (\{z = z_0\} \cup \{z = L_z - z_0\}). \tag{2.17}$$

The modeling above introduces the following boundary value problem:

(2.18)
$$\left\{\begin{array}{rcll} (\overline{\mathbf{v}}\cdot\nabla)\,\overline{\mathbf{v}} - \nu\Delta\mathbf{v} - \nabla\cdot(\nu_t(k))\,D\overline{\mathbf{v}}) + \nabla p &=& \mathbf{f} & \text{in } \mathrm{Om}_c,\\ \nabla\cdot\overline{\mathbf{v}} &=& 0 & \text{in } \mathrm{Om}_c,\\ \overline{\mathbf{v}}\cdot\nabla k - \mu\Delta k - \nabla\cdot(\mu_t(k)\nabla k) &=& \nu_t(k)|D\overline{\mathbf{v}}|^2 - \ell^{-1}k\sqrt{|k|} & \text{in } \mathrm{Om}_c,\\ -[(2\nu+\nu_t(k))D\overline{\mathbf{v}}\cdot\mathbf{n}]_\tau &=& \alpha_v|\overline{\mathbf{v}}|\overline{\mathbf{v}} & \text{on } G_c,\\ \overline{\mathbf{v}}\cdot\mathbf{n} &=& 0 & \text{on } G_c,\\ -(\mu+\mu_t(k))\nabla k\cdot\mathbf{n} &=& \alpha_k k\sqrt{|k|} & \text{on } G_c, \end{array}\right.$$

with periodic boundary conditions in the x and y axes, as defined by (2.2). Roughly speaking the structure of the momentum equation is

$$\text{transport+ viscosity + eddy viscosity + pressure = source}$$

to which the incompressibility constraint and the wall law are added. The structure of the equation for the TKE is

$$\text{transport+ diffusion + eddy diffusion = production of TKE - dissipation}$$

to which the new boundary condition is added.

Remark 2.2. *We have added a diffusion term in the equation for the TKE to avoid degeneration issues in the TKE part of the system, where $\mu > 0$ is a small stabilizing mathematical parameter.*

Remark 2.3. *In the context of the modeling assumptions of this section, the wall law* (1.3) *becomes*

$$(2\nu+\nu_t)\frac{\partial\overline{u}}{\partial z} = \alpha_v\overline{u}^2 \quad at \quad z = z_0, \tag{2.19}$$

$$(2\nu+\nu_t)\frac{\partial\overline{u}}{\partial z} = -\alpha_v\overline{u}^2 \quad at \quad z = L_z - z_0. \tag{2.20}$$

Remark 2.4. *The coefficients $\alpha_v > 0$ and $\alpha_k > 0$ involved in the boundary conditions of* (2.18) *must be set. This point is discussed in section 5.1 below.*

3 Mathematical analysis of the NSTKE model

3.1 Brief state of the art

The goal of this section is to analyse the mathematical structure of the system (2.18), that is the NSTKE model we have introduced above. We start by recalling some notable bibliography facts about NSTKE models. The question is whether the NSTKE model considered in this paper has a structure similar to those studied previously.

It was first studied by Lewandowski [30], where $\Omega \subset \mathbb{R}^d$ $(d = 2, 3)$ is a smooth bounded domain, with homogeneous boundary condition in the whole boundary of Ω, that is $\overline{\mathbf{v}}|_{\partial\Omega} = 0$ and $k|_{\partial\Omega} = 0$, and where ν_t and μ_t are bounded continuous functions of k. Steady state and evolutionary cases were considered in this paper, in which various existence and stability results are proved.

In Bulíček-Lewandowski-Málek [13], the model was studied in $\Omega \subset \mathbb{R}^3$, $\overline{\mathbf{v}}$ satisfies the (linear) Navier Law at $\partial\Omega$, k satisfies mixed homogeneous Dirichlet/Neumann boundary condition at $\partial\Omega$, ν_t and μ_t are continuous functions of k, with growth condition at infinity, covering the case $\nu_t, \mu_t = O\left(k^{1/2}\right)$. In this paper, the k-equation is replaced by the

equation for the total energy $e = 1/2|\overline{\mathbf{v}}|^2 + k$, and the existence of a weak solution to the $(\overline{\mathbf{v}}, p, e)$ system is proved.
In Chacon-Lewandowski [15], we have studied the NSTKE model in $\Omega \subset \mathbb{R}^3$ with the boundary conditions (1.3) (wall law) and (1.4) ($k_{\partial\Omega} = |\overline{\mathbf{v}}|^2$) at the whole boundary. To carry out this study, we have set $k' = k - |\overline{\mathbf{v}}|^2$ and considered the equation for k' in place of that for k. The advantage is that k' satisfies an homogeneous Dirichlet boundary conditions at $\partial\Omega$, suggesting that the method developed in Lewandowski [30] might be adapted. The disadvantage is that additional coupling terms appear in the equation for k'.
In the steady state case, we have proved in Chacon-Lewandowski [15, Chapters 7] the existence of a weak solution to the $(\overline{\mathbf{v}}, \overline{p}, k')$ system when $\nu_t = \nu_t(k)$ and $\mu_t = \mu_t(k)$ are continuous bounded function of k, by a very long and technical proof. When $\nu_t, \mu_t = O\left(k^{1/2}\right)$ at infinity, we still get an existence result when the equality in the k' equation is replaced by a variational inequality. The method fails in the evolutionary case, which still remains an open problem. In this evolutionary case, we have been able to obtain existence results when $k|_{\partial\Omega} = 0$ and $\overline{\mathbf{v}}$ satisfies the wall law (1.3).
In comparison with the former studies, the boundary value problem (2.18) is characterized by

i) mixed boundary conditions, in the sense that they are periodic in the $x - y$ axes, and of flux type in the z-axis (wall law, Neumann),

ii) the non linear Neumann boundary condition (2.14) for k in the z axis.

We will show in the next subsections how the NSTKE model (2.18) studied in this paper, can be put in an abstract form similar to those studied previously. Therefore the previous results, in particular those in Chacon-Lewandowski [15], can be applied to it, in order to get the existence of weak solutions as stated in Theorem 3.1 below.

From now and throughout the rest of the paper we write $\mathbf{v}$ instead of $\overline{\mathbf{v}}$ for the simplicity.

3.2 Variational formulation process

3.2.1 Truncation of the eddy coefficients

We focus to the boundary value problem (2.18), for a given mixing length ℓ and when the eddy viscosity and diffusion are bounded, which corresponds to the typical case

$$\mu_t(k) = T_n(C_v \ell \sqrt{k}), \quad \nu_t(k) = T_n(C_k \ell \sqrt{k}), \tag{3.1}$$

where T_N is the truncation fonction given by

$$T_n(x) = x \quad \text{if } |x| \leq n, \quad T_n(x) = n\frac{x}{|x|} \text{if } |x| \geq N. \tag{3.2}$$

Formally, these eddy coefficients converge to those initially given by (1.2) when $n \to \infty$. We will come back to this passage to the limit in the subsection 3.7 below.

3.2.2 Abstract writing of the system

A weak solution is the solution of a given variational problem. The main difficulty is to find out what is the appropriate variational problem that corresponds to the system (2.18), which combines PDE's and boundary conditions.

We first write (2.18) in its abstract form, which integrates by the mean of operators, the PDE's and the boundary conditions in single equations in the following way.

— Momentum equation:

$$\underbrace{B(\mathbf{v},\mathbf{v})}_{tansport}+\underbrace{A(\mathbf{v})}_{viscosity}+\underbrace{S(k;\mathbf{v})}_{eddy\,viscosity}+\underbrace{G(\mathbf{v})}_{boundary\,term}+\nabla p=\mathbf{f}, \tag{3.3}$$

together with the incompressibilty constraint.

— TKE Equation:

$$\underbrace{B_e(\mathbf{v},k)}_{transport}+\underbrace{A_e(k)}_{diffusion}+\underbrace{S_e(k;k)}_{eddy\,diffusion}+\underbrace{G_e(k)}_{boundary\,term}=\underbrace{P(\mathbf{v},k)}_{production\,of\,TKE}-\underbrace{\varepsilon(k)}_{dissipation} \tag{3.4}$$

where we have set:

$$P(\mathbf{v},k)=\nu_t(k)|D\mathbf{v}|^2,\quad \varepsilon(k)=\ell^{-1}k\sqrt{|k|}. \tag{3.5}$$

Once this is done, we are in order to introduce the following dual operators, where $(\mathbf{w},q,l)$ is what we call the test vector and $(\cdot,\cdot)$ denotes appropriate duality products that we will define later:

(3.6)

transport operators:	$b(\mathbf{v};\mathbf{v},\mathbf{w})=(B(\mathbf{v},\mathbf{v}),\mathbf{w}),$	$b_e(\mathbf{v};k,l)=(B_e(\mathbf{v},k),l),$
viscosity/diffusion operators:	$a(\mathbf{v},\mathbf{w})=(A(\mathbf{v}),\mathbf{w}),$	$a_e(k,l)=(A_e(k),l),$
eddy operators:	$s(k;\mathbf{v},\mathbf{w})=(S(k;\mathbf{v}),\mathbf{w}),$	$s_e(k;k,l)=(S_e(k;k),l),$
boundary terms:	$g(\mathbf{v},\mathbf{w})=(G(\mathbf{v}),\mathbf{w}),$	$g_e(\mathbf{v},\mathbf{w})=(G_e(\mathbf{v}),\mathbf{w}).$

The determination of these operators yields the variational formulations of the NSTKE model that we study. The solutions to the variational problem which we obtain, are weak solutions of this model.

3.2.3 Expression of the operators

The method for determining the variational formulation of the PDE's system with boundary conditions (2.18), is to take the dot product of the momentum equation by $\mathbf{w}$, to multiply the TKE equation by l and to integrate by parts. To do so, we need carreful geometrical definitions about the computational domain, restricted to a calculation box called Ω_c and given by:

$$\Omega_c=[0,L_x]\times[0,L_y]\times[z_0,L_z-z_0], \tag{3.7}$$

$$\Gamma_{b,c}=[0,L_x]\times[0,L_y]\times\{z=z_0\}\quad\text{(bottom)}, \tag{3.8}$$

$$\Gamma_{t,c}=[0,L_x]\times[0,L_y]\times\{z=L_z-z_0\}\quad\text{(top)}, \tag{3.9}$$

$$\Gamma_c=\Gamma_{b,c}\cup\Gamma_{t,c}\quad\text{(bottom}\cup\text{top)}. \tag{3.10}$$

Following a standard procedure in CFD, the transport operators are symmetrized in order to verify the identities

$$b(\mathbf{v},\mathbf{v},\mathbf{v})=0,\quad b_e(\mathbf{v},k,k)=0, \tag{3.11}$$

in particular

$$b(\mathbf{v},\mathbf{v},\mathbf{w}) = \frac{1}{2}\left(\int_{\Omega_c}(\mathbf{v}\cdot\nabla)\mathbf{v}\cdot\mathbf{w} - \int_{\Omega_c}(\mathbf{v}\cdot\nabla)\mathbf{w}\cdot\mathbf{v}\right). \tag{3.12}$$

as well as

$$b_e(\mathbf{z};k,l) = \frac{1}{2}\left[\int_{\Omega_c}(\mathbf{v}\cdot\nabla k)l - (\mathbf{v}\cdot\nabla l,k)\right], \tag{3.13}$$

We show in Lemma 3.1 that these operators match well with the transport involved in the model, because of the incompressibility constraint.
We also will show in the next subsections that the natural definition for the other operators are the following:

$$\begin{cases} a(\mathbf{v},\mathbf{w}) = \nu\displaystyle\int_{\Omega_c}\nabla\mathbf{v}:\nabla\mathbf{w}, & a_e(k,l) = \mu\displaystyle\int_{\Omega_c}\nabla k\cdot\nabla l, \\ s(k;\mathbf{v},\mathbf{w}) = \displaystyle\int_{\Omega_c}\nu_t(k)D\mathbf{v}:D\mathbf{w}, & s_e(k;q,l) = \displaystyle\int_{\Omega_c}\mu_t(k)\nabla q\cdot\nabla l, \\ g(\mathbf{v},\mathbf{w}) = \alpha_v\displaystyle\int_{\Gamma_c}\mathbf{v}|\mathbf{v}|\mathbf{w}, & g_e(k,l) = \alpha_k\displaystyle\int_{\Gamma_c}k\sqrt{k}\,l. \end{cases} \tag{3.14}$$

We notice that when the fields $(\mathbf{v},k)$ and $(\mathbf{w},l)$ are of class C^1 in the computational domain, the integrals involved in the definitions (3.12), (3.13) and (3.14) are well defined.

3.2.4 Toward a variational formulation

The machinery behind the determination of weak solutions is based on functional analysis, the main results of which are verified in Banach spaces, whose norms are L^p norms of the functions and/or their derivative. However C^1 functions spaces are not Banach spaces for such norms, and we must use Lebesgue and Sobolev spaces. From there, the challenge is the determination of the appropriate spaces E_1, F_1 and G_1 where to look for the unknowns, and E_2, F_2 and G_2 where to take the vector tests, so that the variational formulation of our problem gets:

Find $(\mathbf{v},p,k)\in E_1\times F_1\times G_1$ such that for all $(\mathbf{w},q,l)\in E_2\times F_2\times G_2$, (3.15)

1 Momentum equation:

$$\underbrace{b(\mathbf{v};\mathbf{v},\mathbf{w})}_{tansport} + \underbrace{a(\mathbf{v},\mathbf{w})}_{viscosity} + \underbrace{s(k;\mathbf{v},\mathbf{w})}_{eddy\,viscosity} + \underbrace{g(\mathbf{v},\mathbf{w})}_{boundary\,term} - \underbrace{(p,\nabla\cdot\mathbf{w})}_{pressure} = \underbrace{(\mathbf{f},\mathbf{w})}_{source\,term} \tag{3.16}$$

2) incompressibilty condition:

$$(q,\nabla\cdot\mathbf{v}) = 0, \tag{3.17}$$

3) TKE Equation:

$$\underbrace{b_e(\mathbf{v};k,l)}_{transport} + \underbrace{a_e(k,l)}_{diffusion} + \underbrace{s_e(k;k,l)}_{eddy\,diffusion} + \underbrace{g_e(k,l)}_{boundary\,term} = \underbrace{(P(\mathbf{v},k),l)}_{production\,term} - \underbrace{(\varepsilon(k),l)}_{dissipation\,term}. \tag{3.18}$$

This formulation will be completed by the subsection 3.6. The difficulty is to carrefully construct the functional spaces involved in the formulation, which is the aim of the next subsections.

3.3 Functional space where to look for the velocity

From now, the working assumptions are the following:

$$\left\{\begin{array}{l}\text{(i) The mixing length } \ell = \ell(\mathbf{x}) \text{is a given strictly non negative bounded continuous function,}\\ \text{(ii) } \nu > 0,\ \mu > 0,\ \alpha_v > 0,\ \alpha_k > 0 \text{ are constants,}\\ \text{(iii) the eddy viscosity } \nu_t = \nu_t(k) \geq 0 \text{ and } \mu_t = \mu_t(k) \geq 0 \\ \text{are continuous bounded function of } k.\end{array}\right. \tag{3.19}$$

The goal of this section is to carrefully construct the Sobolev space where we will look for the velocity, which will be defined as the product of Sobolev spaces. What makes the problem difficult is the fact that we work with mixed boundary conditions for the velocity $\mathbf{v}$, which is naturally broken down into its horizontal component $\mathbf{v}_h = (v_x, v_y)$ and its vertical component v_z, each component to be treated differently.

3.3.1 Energy balance

The starting point of the process is the energy balance, that we obtain by taking formally $\mathbf{w} = \mathbf{v}$ as test in equation (3.16), combined with the constraint $\nabla \cdot \mathbf{v} = 0$ and the relation (3.11), so that the pressure and the transport terms vanish. Therefore the energy balance is:

$$\nu \int_{\Omega_c} |\nabla \mathbf{v}|^2 + \int_{\Omega_c} \nu_t(k) |D\mathbf{v}|^2 + \alpha_v \int_{\Gamma_c} |\mathbf{v}|^3 = (\mathbf{f}, \mathbf{v}), \tag{3.20}$$

which indicates that we have to construct a space that looks like $W^{1,2}(\Omega_c)^3$, with the $x-y$ periodicity and the fact that $\mathbf{v} \cdot \mathbf{n} = v_z = 0$ at Γ_c in addition. Moreover, to take advantage of the energy balance (3.20), this space should be normed by the norm[4]

$$N(\mathbf{v}) = \left(\int_{\Omega_c} |\nabla \mathbf{v}|^2 \right)^{1/2} + \left(\int_{\Gamma_c} |\mathbf{v}|^2 \right)^{1/2}, \tag{3.21}$$

which is equivalent to the usual norm on the space $W^{1,2}(\Omega_c)^3$,

$$||\mathbf{v}||_{1,2,\Omega_c} = \left(\int_{\Omega_c} |\nabla \mathbf{v}|^2 \right)^{1/2} + \left(\int_{\Omega_c} |\mathbf{v}|^2 \right)^{1/2}, \tag{3.22}$$

see in Bulíček-Málek-Rajagopal [14].
As we know from the Hölder inequality that

$$\int_{\Gamma_c} |\mathbf{v}|^2 \leq \text{meas}(\Gamma_c)^{1/3} \left(\int_{\Gamma_c} |\mathbf{v}|^3 \right)^{2/3}, \tag{3.23}$$

then the energy balance (3.20) yields, because ν_t is nonnegative, $\alpha_v, \nu > 0$,

$$N(\mathbf{v}) \leq C(\alpha_v, \nu, \Omega_c) ||\mathbf{f}||, \tag{3.24}$$

for the norm of $\mathbf{f}$ in the dual space of $W^{1,2}(\Omega_c)^3$.

[4]For the simplicity and when no risk of confusion occurs, we indentify $\mathbf{v}$ at Γ_c to his trace, without changing the notation. When necessary, we will use the usual notation for the trace, that is $tr\mathbf{v}$.

Remark 3.1. *Let $1 \leq p < \infty$. The trace operator is surjective from $tr = H^1_\pi \to W^{1,1-1/p}(\Gamma_c)$. Therefore, following Bulíček-Málek-Rajagopal [14], it also can be seen that, given any $1 \leq q \leq q^{**}$, where q^{**} is the critical exponent exponent in the Sobolev injection $W^{1,1-1/p}(\Gamma_c) \hookrightarrow L^q(\Omega_c)$, the norm given by*

$$||\psi|| = \left(\int_{\Omega_c} |\nabla\psi|^p\right)^{1/p} + \left(\int_{\Gamma_c} |\psi|^q\right)^{1/q} \tag{3.25}$$

is a norm on H^1_π equivalent to the usual one.

3.3.2 $x-y$ periodic Lebesgue and Sobolev spaces

Lebesgue and Sobolev spaces are oftently constructed as the completion of C^∞-function spaces. In order to take the $x-y$ periodicity into account, we consider the following space:

$$\begin{aligned}\mathcal{W} = \big\{&\psi \in C^\infty(\mathbb{R}^2 \times [z_0, L_z - z_0], \mathbb{R}) \text{ s.t.} \\ &\forall\,(m,n) \in \mathbb{N}^2,\ \forall\,(x,y,z) \in \Omega_c,\ \psi(x + nL_x, y + mL_y, z) = \psi(x,y,z)\big\},\end{aligned} \tag{3.26}$$

which means the smooth function defined in the strip $z_0 \leq z \leq L_z - z_0$, periodic in the (x,y)-axes by the $[0,L_x] \times [0,L_y]$ box.

Given any $\psi \in \mathcal{W}$, we still denote by ψ its restriction to Ω_c, so far no risk of confusion occurs. It can be easily checked that the standard L^p norm on Ω_c and the norm N given by (3.21), are norms on $\mathcal{W}$, because of the periodicity.
We define:

- The space L^p_π, the completion of $\mathcal{W}$ with respect to the L^p norm on Ω_c,
- The space H^1_π, the completion of $\mathcal{W}$ with respect to the norm N given by (3.21).

From now, we denote by $||\cdot||_{s,p,\Omega_c}$ the standard $W^{s,p}$ norm on Ω_c. In particular, $||\cdot||_{0,p,\Omega_c}$ is the L^p norm. We also will make no distinction between the norm N given by (3.21) and the usual $W^{1,2}$ norm given (3.22), which will be both be denoted by $||\cdot||_{1,2,\Omega_c}$ so far no risk of confusion occurs.

We also will consider the $W^{1,p}_\pi$, which is the completion of $\mathcal{W}$ with respect of the $W^{1,p}$ norm on Ω_c.

3.3.3 Vertical homogeneous space to treat the vertical component.

In order to treat the fact that $v_z = 0$ at Γ_c, we will need the following space:

$$\begin{aligned}\mathcal{W}_0 = \{&\psi \in \mathcal{W} \text{ s.t.} \\ &\exists\,\delta > 0,\ \forall\,(x,y) \in \mathbb{R}^2,\ \forall z \in [z_0, z_0+\delta] \cup [L_z - z_0 - \delta, L_z - z_0], \\ &\psi(x,y,z) = 0\}.\end{aligned} \tag{3.27}$$

In other word, $\mathcal{W}_0$ is the set of functions in $\mathcal{W}$ vanishing in a neighbourhood of the bottom $z = z_0$ and the top $z = L_z - z_0$.

Let $H^1_{\pi,0}$ denotes the closure of $\mathcal{W}_0$ in H^1_π.

By simply adapting a standard argument to this situation it is easy checked that given any $\psi \in W^{1,2}_{\pi}$, then

$$\psi \in H^1_{\pi,0} \quad \text{if and only if} \quad \psi|_{\Gamma_c} = 0,$$

see for instance in Brézis [12]. Moreover, the following Poincaré's inequality holds

$$\forall\, \psi \in H^1_{\pi,0}, \quad ||\psi||_{0,2,\Omega_c} \leq C_{\Omega_c} ||\nabla \psi||_{0,2,\Omega_c}, \tag{3.28}$$

where C_{Ω_c} is a constant that only depends on Ω_c. Note that in view of the geometry of Ω_c, a straightforward calculation using Fubini's theorem allows to check that (3.28) can be improved by:

$$\forall\, \psi \in W^{1,2}_{\pi,0}, \quad ||\psi||_{0,2,\Omega_c} \leq C_{L_z} ||\frac{\partial \psi}{\partial z}||_{0,2,\Omega_c}, \tag{3.29}$$

3.3.4 Space for the velocity.

The boundary condition $\overline{\mathbf{v}} \cdot \mathbf{n} = 0$ at $z = z_0$ and $z = L_z - z_0$ must be considered in the functional setting. Let $\mathbf{w} = (w_x, w_y, w_z)$ be a vector field defined over $\mathbb{R}^2 \times [z_0, L_z - z_0]$ that satisfies

$$\mathbf{w} \cdot \mathbf{n}|_{z=z_0} = \mathbf{w} \cdot \mathbf{n}|_{z=L_z - z_0} = 0,$$

then

$$w_z(x, y, z_0) = w_z(x, y, L_z - z_0) = 0.$$

In other words, $w_z|_{\Gamma_c} = 0$. Therefore, according to this point and from above, we are led to seek for the velocity in the space

$$W = H^1_{\pi} \times H^1_{\pi} \times H^1_{\pi,0}. \tag{3.30}$$

3.4 Properties of the operators

From now, the source term $\mathbf{f}$ in (2.18) is in the dual space W'. We aim in this section to justify the introduction of the operators given by (3.14), to study their main properties, as well as to study the properties of the transport operators.

3.4.1 Turbulent operator

In this section, we construct simultaneously the eddy viscosity-diffusion operators $a(\mathbf{v}, \mathbf{w})$ and $a_e(k, l)$, and the boundary terms $g(\mathbf{v}, \mathbf{w})$ and $g_e(k, l)$ by the Stokes formula.

Let $A = A(\mathbf{x})$ denotes a C^1 (x, y)-periodic matrix, positive definite uniformly in $\mathbf{x} = (x, y, z) \in \Omega_c = \mathbb{R}^2 \times [z_0, L_z - z_0]$, that is

$$\forall\, \mathbf{u} \in \mathbb{R}^3, \quad \forall\, \mathbf{x} \in \Omega_c, \quad (A(\mathbf{x})\mathbf{u}, \mathbf{u}) \geq \nu |\mathbf{u}|^2. \tag{3.31}$$

Let $\psi, \phi \in \mathcal{W}$. By the Stokes formula over Ω_c, which is a Lipchitz domain, we have

$$\int_{\Omega_c} -\nabla \cdot (A \nabla \psi)\phi = -\int_{\partial\Omega_c} \phi A \nabla \psi \cdot \mathbf{n} + \int_{\Omega_c} A \nabla \psi \cdot \nabla \phi. \tag{3.32}$$

Using the notations of figure 2, we decompose the integral on $\partial\Omega_c$ as

$$\int_{\partial\Omega_c} = \int_{\Gamma_c} + \int_{\Gamma_e} + \int_{\Gamma_s} + \int_{\Gamma_{lg}} + \int_{\Gamma_{lr}} \tag{3.33}$$

We have: $\mathbf{n}|_{\Gamma_e} = -\mathbf{n}|_{\Gamma_s}$ and $\mathbf{n}|_{\Gamma_{lg}} = -\mathbf{n}|_{\Gamma_{lr}}$. As $\phi A\nabla\psi$ is a C^1 function, periodic in the (x, y)-axes, we also have $\phi A\nabla\psi|_{\Gamma_e} = \phi A\nabla\psi|_{\Gamma_s}$ as well as $\phi A\nabla\psi|_{\Gamma_{lg}} = \phi A\nabla\psi|_{\Gamma_{lr}}$. Therefore, aside the term on Γ_c, all other terms in the boundary integral (3.33) are vanishing, hence (3.32) yields

$$(-\nabla\cdot(A\nabla\psi)\phi,\phi) = \int_{\Omega_c} -\nabla\cdot(A\nabla\psi)\phi = -\int_{\Gamma_c}\phi A\nabla\psi\cdot\mathbf{n} + \int_{\Omega_c} A\nabla\psi\cdot\nabla\phi. \tag{3.34}$$

Unfortunately, the operator

$$\begin{cases} \mathcal{W} \to L^p(\Gamma_c), \\ \psi \to \mathrm{tr}(A\nabla\psi)\cdot\mathbf{n} \end{cases}$$

is not bounded, whatever the choice of $p \geq 1$. Therefore, Formula (3.34) cannot be extended for any ψ and ϕ in $W^{1,p}_\pi$ spaces. However, the structure of our problem suggests to introduce the following. Let $F : \mathbb{R} \to \mathbb{R}$ be a function which satisfies the growth condition

$$|F(\psi)| \leq C(1 + |\psi|^q), \tag{3.35}$$

for some q that be specified later, and let us consider

$$\mathcal{M}_F = \{\psi \in \mathcal{W};\ \mathrm{tr}(A\nabla\psi)\cdot\mathbf{n} = -F(\psi)\}.$$

Let M_F denotes the adherence of $\mathcal{M}_F$ with respect to the $W^{1,p}$ topology. For $\psi \in M_F$, $\phi \in W^{1,p'}_\pi$, the equality (3.34) becomes

$$(-\nabla\cdot(A\nabla\psi)\phi,\phi) = \int_{\Gamma_c}\phi F(\psi) + \int_{\Omega_c} A\nabla\psi\cdot\nabla\phi. \tag{3.36}$$

We observe on one hand that as $\nabla\psi \in L^p(\Omega_c)$ and $\nabla\phi \in L^{p'}(\Omega_c)$, the volume integral in (3.36) is also well defined as soon as $A \in L^{p'}(\Omega_c)$. On a second hand, straightforward calculations based on Hölder and Sobolev inequalities, yield the following rules for the right choice of q to make the boundary integral well defined in (3.36):

$$\begin{cases} \text{if } 1 \leq p < 3/2, \quad q \leq p^{\star\star} = \dfrac{2p}{3-p} = q_c, \\ \text{if } p = 3/2, \quad q < 2 = q_c, \\ \text{if } 3/2 < p < 3, \quad q \leq \dfrac{3}{3-p} = q_c. \end{cases} \tag{3.37}$$

In the equation for $\overline{\mathbf{v}}$[5], $A = (2\nu + \nu_t(k))\mathrm{Id}$, $p = 2$ and

$$F(\overline{\mathbf{v}}) = \alpha_v|\overline{\mathbf{v}}|\overline{\mathbf{v}}. \tag{3.38}$$

then $q = 2$ and $q_c = 3$. This case is well covered by the classification (3.37). In the k-equation, $A = (\mu + \mu_t(k))\mathrm{Id}$, $p = 3/2^-$,

$$F(k) = \alpha_k k\sqrt{|k|}, \tag{3.39}$$

then $q = 3/2$ and $q_c = 2$, which is also well covered by the classification (3.37).

[5]Things are a little bit more technical with vector fields and laws such as (1.3), but the calculation and the final result are similar to the scalar case, changing ∇ by D, and thus we will not repeat it.

3.4.2 Transport operators

Let's remember that as we are not working with a space of free divergence field, following Chacon-Lewandowski [15, Chapter 6], we use the transport operator $b(\mathbf{z};\mathbf{v},\mathbf{w})$ in the momentum equation, defined by

$$b(\mathbf{z};\mathbf{v},\mathbf{w}) = \frac{1}{2}\left(\int_{\Omega_c}(\mathbf{z}\cdot\nabla)\mathbf{v}\cdot\mathbf{w} - \int_{\Omega_c}(\mathbf{z}\cdot\nabla)\mathbf{w}\cdot\mathbf{v}\right). \tag{3.40}$$

By similar calculations as those carried out in section (3.4.1) and arguments of the proof of Lemma 6.3 in Chacon-Lewandowski [15], we easily get:

Lemma 3.1. *The form $(\mathbf{z},\mathbf{v},\mathbf{w}) \to b(\mathbf{z};\mathbf{v},\mathbf{w})$ verifies the following properties.*

i) b is trilinear and continuous on $(H^1_\pi)^3$, then on W, and in particular,

$$\forall\, \mathbf{z},\ \mathbf{v},\ \mathbf{w} \in (H^1_\pi)^3, \quad |b(\mathbf{z};\mathbf{v},\mathbf{w})| \le C\,\|\mathbf{z}\|_{1,2,\Omega_c}\,\|\mathbf{v}\|_{1,2,\Omega_c}\,\|\mathbf{w}\|_{1,2,\Omega_c}, \tag{3.41}$$

for some constants C only depending on Ω.

ii) b is antisymmetric,

$$\forall\, \mathbf{z},\ \mathbf{v},\ \mathbf{w} \in (H^1_\pi)^3, \quad b(\mathbf{z};\mathbf{v},\mathbf{w}) = -b(\mathbf{z};\mathbf{w},\mathbf{v}), \tag{3.42}$$

iii) we also have

$$\forall\, \mathbf{z},\ \mathbf{w}\ \in (H^1_\pi)^3, \quad b(\mathbf{z};\mathbf{w},\mathbf{w}) = 0. \tag{3.43}$$

iv) For any $\mathbf{z} \in W$ such that $\nabla\cdot\mathbf{z} = 0$ (in L^2_π), we have

$$\forall\, \mathbf{v},\ \mathbf{w}\ \in (H^1_\pi)^3, \quad b(\mathbf{z};\mathbf{v},\mathbf{w}) = \int_{\Omega_c}(\mathbf{z}\cdot\nabla)\,\mathbf{v}\cdot\mathbf{w}, \tag{3.44}$$

as well as

$$\forall\, \mathbf{w}\ \in (H^1_\pi)^3, \quad b(\mathbf{z};\mathbf{z},\mathbf{w}) = -\int_{\Omega_c}\mathbf{z}\otimes\mathbf{z} : \nabla\mathbf{w}. \tag{3.45}$$

The transport operator b_e involved in the TKE equation, that is

$$b_e(\mathbf{z};k,l) = \frac{1}{2}\left[(\mathbf{z}\cdot\nabla k, l) - (\mathbf{z}\cdot\nabla l, k)\right], \tag{3.46}$$

where[6] $\int_{\Omega_c}\phi\psi = (\phi,\psi)$, satisfies the same properties as the operator b. Moreover, following Stampacchia [49], we also have for any C^1 piecewise function H that vanishes at 0,

$$b_e(\mathbf{v},k,H(k)) = 0. \tag{3.47}$$

We have just taken an important step because, from the above, we are now able to specify the spaces for the velocity and the pressure and the corresponding tests introduced in the subsection 3.2.4, by setting

$$E_1 = E_2 = W, \quad F_1 = F_2 = L^2_\pi, \tag{3.48}$$

where W is specified by (3.30).

[6] More generally, given any Banach space E, $\psi \in E$, $\phi \in E'$, then so far no risk of confusion occurs, (ϕ,ψ) denotes the duality product between ϕ and ψ.

3.5 Treatment of the TKE equation

Basically, the TKE-equation (3.18) is an transport-diffusion equation with a right hand side in L^1 (see for instance Boccardo-Diaz-Giachetti-Murat, [9], Boccardo-Murat [11] and in Lewandowski [29, Chapter 5]). Indeed, we deduce from the energy balance (3.20) combined with the inequality (3.23),

$$C||\mathbf{v}||_{1,2,\Omega} + \int_{\Omega_c} \nu_t(k))|D\mathbf{v}|^2 \leq (\mathbf{f}, \mathbf{v}), \tag{3.49}$$

where C is a constant that depend on α_v, ν and Γ_c.
Therefore, by Young inequality, (3.49) yields

$$\frac{C}{2}||\mathbf{v}||^2_W + \int_{\Omega_c} \nu_t(k)|D\mathbf{v}|^2 \leq \frac{1}{2C}||\mathbf{f}||_{W'}. \tag{3.50}$$

Hence the production term $P(k, \mathbf{v}) = \nu_t(k)|D\mathbf{v}|^2$ does belong to $L^1(\Omega_c)$.

Lemma 3.2. *For all $1 \leq q < 3/2$, there exists a constant $C_q = C_q(\alpha_v, \nu, \Omega_c, ||\mathbf{f}||_{W'})$ such that any solution k to (3.18) satisfies the a priori estimate*

$$||k||_{1,q,\Omega_c} \leq C_q. \tag{3.51}$$

Proof. The proof is divided into two steps. We first find a uniform estimate of $||\mathrm{tr}k||_{0,3/2,\Gamma_c}$. Then we derive from the Boccardo-Gallouët [10] inequality an estimate of $||\nabla k||_{0,q,\Omega}$ that yields the conclusion.

Step 1. Estimate at the boundary. Given any $\varepsilon > 0$, let S_ε be the odd function defined by

$$\begin{cases} S_\varepsilon(x) = \varepsilon^{-1}x & \text{if } x \in [0, \varepsilon], \\ S_\varepsilon(x) = 1 & \text{if } x \in [\varepsilon, \infty[. \end{cases} \tag{3.52}$$

We chose $l = S_\varepsilon(k)$ as test in (3.18), taking into account that:

- by (3.47), $b_e(\mathbf{v}, k, S_\varepsilon(k)) = 0$,
- because $S'_\varepsilon \geq 0$ and $\mu_t \geq 0$, $a_e(k, S_\varepsilon(k) \geq 0$,
- $(\varepsilon(k), S_\varepsilon(k)) = \varepsilon^{-1} \displaystyle\int_{|k|\leq 1/\varepsilon} \ell^{-1}|k|^{3/2} + \int_{|k|\geq 1/\varepsilon} \ell^{-1}|k|^{1/2} \geq 0$,
- $|S_\varepsilon(k)| \leq 1$,

we have by (3.50),

$$\int_{\Omega_c} S'_\varepsilon(k)|\nabla k|^2 + \alpha_k \int_{\Gamma_c} k|k|^{\frac{1}{2}} S_\varepsilon(k) \leq \int_{\Omega_c} P(\mathbf{v}, k)S_\varepsilon(k) \leq C||\mathbf{f}||_{W'} \tag{3.53}$$

As S_ε is non decreasing, $S'_\varepsilon(k)|\nabla k|^2 \geq 0$. Hence (3.53) yields

$$\alpha_k \int_{\Gamma_c} k|k|^{\frac{1}{2}} S_\varepsilon(k) \leq C||\mathbf{f}||_{W'}, \tag{3.54}$$

which gives by Fatou's Lemma, since $S_\varepsilon(k) \to \mathrm{sign}(k)$ where $k \neq 0$ as $\varepsilon \to 0$,

$$\int_{\Gamma_c \cap \{k\neq 0\}} |k|^{\frac{3}{2}} \leq \liminf_{\varepsilon\to 0} \int_{\Gamma_c\cap\{k\neq 0\}} k|k|^{\frac{1}{2}} S_\varepsilon(k) \leq C||\mathbf{f}||_{W'},$$

leading to

$$\int_{\Gamma_c} |k|^{\frac{3}{2}} \leq C||\mathbf{f}||_{W'}, \tag{3.55}$$

hence a uniform $L^{3/2}$ estimate for k at Γ_c.

Step 2. Estimate inside Ω. Given any $n \in \mathbb{N}$, let $H_n : \mathbb{R} \to \mathbb{R}$ be the odd continuous Lipchitz function defined by

$$\begin{cases} H_n(x) = 0 & \text{if } x \in [0, n], \\ H_n(x) = x - n & \text{if } x \in [n, n+1], \\ H_n(x) = 1 & \text{if } x \in [n+1, \infty[. \end{cases} \tag{3.56}$$

Taking $H_n(k)$ as test in (3.18) yields, by similar arguments,

$$\int_{\Omega_c} H_n'(k)|\nabla k|^2 + \alpha_k \int_{\Gamma_c} k|k|^{\frac{1}{2}} H_n(k) \leq \int_{\Omega_c} P(k, \mathbf{v}) H_n(k) \leq C||\mathbf{f}||_{W'} \tag{3.57}$$

As H_n is odd, $k|k|^{\frac{1}{2}} H_n(k) \geq 0$. Therefore, (3.49) yields

$$\int_{n \leq |k| \leq n+1} |\nabla k|^2 \leq C||\mathbf{f}||_{W'}. \tag{3.58}$$

From this estimate, we can use the result of Boccardo-Gallouët [10] turnkey. Therefore, for all $q < 3/2$, for all $\varepsilon > 0$, there exists C_ε (that depends on q and $C||\mathbf{f}||_{W'}$), such that

$$||\nabla k||^q_{0,q,\Omega_c} \leq C_\varepsilon + \varepsilon ||k||^{\frac{q^\star(2-q)}{2}}_{0,q^\star,\Omega_c}. \tag{3.59}$$

Hence according to Remark 3.1 combined with the Sobolev inequality and (3.55),

$$\begin{aligned} ||\nabla k||^q_{0,q,\Omega_c} &\leq C_\varepsilon + \varepsilon S^{\frac{q^\star(2-q)}{2}} (||\nabla k||_{0,q,\Omega_c} + ||\mathrm{tr} k||_{0,3/2,\Gamma_c})^{\frac{q^\star(2-q)}{2}} \\ &\leq C_\varepsilon + \varepsilon S^{\frac{q^\star(2-q)}{2}} (||\nabla k||_{0,q,\Omega_c} + (C||\mathbf{f}||_{W'})^{2/3})^{\frac{q^\star(2-q)}{2}}. \end{aligned} \tag{3.60}$$

The conclusion follows from (3.60) because $q^\star \frac{(2-q)}{2} < q$. □

We set in what follows:

$$W_\pi^{1,\frac{3}{2}^-} = \bigcap_{r<3/2} W_\pi^{1,r}, \quad W_\pi^{1,3^+} = \bigcup_{\rho>3} W_\pi^{1,\rho}, \tag{3.61}$$

which specifies now the space where to look for the TKE k and the corresponding tests.

3.6 Main result

The results above allow to complete the variational problem corresponding to the system (2.18) introduced in the subsection 3.2.4, and to clarify the statement of the main theoretical result in this paper. According from above, the variational formula of subsection 3.2.4 gets:

$$\text{Find } (\mathbf{v}, p, k) \in W \times L^2_\pi \times H_\pi^{1,\frac{3}{2}^-} \text{ s.t. for all } (\mathbf{w}, q, l) \in W \times L^2_\pi \times H_\pi^{1,3^+}, \tag{3.62}$$

$$b(\mathbf{v};\mathbf{v},\mathbf{w}) + a(\mathbf{v},\mathbf{w}) + s(k;\mathbf{v},\mathbf{w}) + g(\mathbf{v},\mathbf{w}) - (p,\nabla\cdot\mathbf{w}) = (\mathbf{f},\mathbf{w}), \tag{3.63}$$

$$(q,\nabla\cdot\mathbf{v}) = 0, \tag{3.64}$$

$$b_e(\mathbf{v};k,l) + a_e(k,l) + s_e(k;k,l) + g_e(k,l) = (P(k,\mathbf{v}) - \varepsilon(k),l). \tag{3.65}$$

Any solution to the variational problem (3.63)-(3.63)-(3.63) is a weak solution to the system (2.18). The calculation carried out before ensures that any strong solution to (2.18) is a weak solution. Conversely, it is easily checked that if $(\mathbf{v},p,k)$ is a weak solution which in addition satisfies $(\mathbf{v},p,k) \in (H^2_\pi)^3 \times H^1_\pi \times H^2_\pi$, and ν_t, μ_t are C^1 functions, then $(\mathbf{v},p,k)$ is also a strong solution to (2.18), and the following holds true:

Theorem 3.1. *Assume that assumptions 3.19 hold. Then System (2.18) has a weak solution* $(\mathbf{v},p,k) \in W \times L^2_\pi \times H^{1,\frac{3}{2}^-}$.

The analysis carried out above shows that the weak formulation of system (2.18) is formulated as that considered in Chacon-Lewandowski [15, Chapter 7], which was one of our goal. Therefore, the proof is similar to that of Theorem 7.1 in Chacon-Lewandowski [15][7]. We use a fixed point method, which requires a compactness property. The main ingredient to get it, is the energy method. Roughly speaking, it consists in proving that given a sequence of solution $(\mathbf{v}_j,p_j,k_j)_{j\in\mathbf{N}}$ to the variational problem (3.62)-(3.63)-(3.64)-(3.65), then from this sequence we can extract a subsequence, still denoted by $(\mathbf{v}_j,p_j,k_j)_{j\in\mathbf{N}}$, which weakly converges to some $(\mathbf{v},p,k)$ in $W \times L^2_\pi \times H^{1,\frac{3}{2}^-}$ and such that

$$\lim_{j\to\infty} P(k_j,\mathbf{v}_j) = P(k,\mathbf{v}) \quad \text{strongly in } L^1_\pi, \tag{3.66}$$

so that we can pass to the limit in the production term, which is the source of difficulty.

Remark 3.2. *It is easily proved by standard arguments that the TKE k is non negative.*

3.7 From bounded to unbounded eddy viscosities

It remains to say some words about the problem of unbounded eddy coefficients raised in the subsection 3.2.1. Any n being given, we can consider

$$\mu_t^n(k) = T_n(C_v\ell\sqrt{k}), \quad \nu_t^n(k) = T_n(C_k\ell\sqrt{k}). \tag{3.67}$$

According to Theorem 3.1, there is a solution $(\mathbf{v}_n,p_n,k_n)$ to the problem with $\mu_t^n(k)$ and $\nu_t^n(k)$ as eddy coefficients. Thereofore, we can prove that from the sequence $(\mathbf{v}_n,p_n,k_n)_{n\in\mathbf{N}}$, we can extract a subsequence, still denoted by $(\mathbf{v}_j,p_j,k_j)_{j\in\mathbf{N}}$, which weakly converges to some $(\mathbf{v},p,k \in W \times L^2_\pi \times H^{1,\frac{3}{2}^-}$. From there, we are able to pass to the limit in the momentum equation, but not in the TKE equation because we are not able to prove that (3.66) is satisfied, and we only obtain a variational inquality, so that the limit satisfies, when $\nu_t = C_v\ell k\sqrt{k}$, $\mu_t = C_k\ell k\sqrt{k}$,

$$\text{for all } (\mathbf{w},q,l) \in W \times L^2_\pi \times H^{1,3^+}_\pi, \tag{3.68}$$

$$b(\mathbf{v};\mathbf{v},\mathbf{w}) + a(\mathbf{v},\mathbf{w}) + s(k;\mathbf{v},\mathbf{w}) + g(\mathbf{v},\mathbf{w}) - (p,\nabla\cdot\mathbf{w}) = (\mathbf{f},\mathbf{w}), \tag{3.69}$$

$$(q,\nabla\cdot\mathbf{v}) = 0, \tag{3.70}$$

$$b_e(\mathbf{v};k,l) + a_e(k,l) + s_e(k;k,l) + g_e(k,l) \le (P(k,\mathbf{v}) - \varepsilon(k),l). \tag{3.71}$$

[7] In fact it is much more simpler in this case, since we do not have many additional terms coming from the boundary condition, in which $\mathbf{v}$ is involved. These terms are replaced by the boundary term $g_e(k,l)$, which is easily treated, just as the term $g(\mathbf{v},\mathbf{w})$ in the $\mathbf{v}$-equation.

It does not seem useful to give more technical development, since in practice k remains bounded, and the turbulent coefficients coincide with their truncated versions for a certain n large enough.

4 Direct Numerical Simulations

We perform and validate in this section several DNS, in order to derive a universal formula for the mixing length ℓ as a function of the frictional Reynolds number

$$Re_\star = \frac{u^\star H}{\nu}, \tag{4.1}$$

the friction velocity $u_\star$ being given by (2.5), $H = L_z/2$. The frictional Reynolds number is the main control parameter in this study. To close the set of parameters, we enforce u to be equal to 1 at $z = H$. We will use the following standard relation between $u_\star$ and $Re_\star$:

$$u_\star = \left(\frac{1}{0.41} \log Re_\star + 5.5 \right)^{-1}, \tag{4.2}$$

which is a byproduct of the log law. Therefore, $Re_\star$ yields $u_\star$ and then ν from (4.1) re-written as

$$\frac{\nu}{u_\star} = \frac{H}{Re_\star}. \tag{4.3}$$

Note that $\nu/u_\star$ is the natural length scale of the flow.

4.1 Settings and results

To begin with, we set data and parameters for the simulations.

i) Software and equations. The direct numerical simulations (DNS) are performed by using the parallelised flow solver Incompact3d (see at `https://www.incompact3d.com/`). The numerical schemes implemented in this software are detailed in Laizet-Lamballais [25], Laizet-Li [26] Lele [28]. The equations, solved in $\Omega = [0, L_x] \times [0, L_y] \times [0, L_z]$, are[8]:

$$\begin{cases} \partial_t \mathbf{v} + \frac{1}{2} \left[\nabla \cdot (\mathbf{v} \otimes \mathbf{v}) + (\mathbf{v} \cdot \nabla)\mathbf{v} \right] - \nabla \cdot (\nu \nabla \mathbf{v}) + \nabla p = \mathbf{f}, \\ \nabla \cdot \mathbf{v} = 0, \\ \mathbf{v}|_{z=0} = \mathbf{v}|_{z=L_z} = 0, \quad \mathbf{v} \text{ periodic in the } x-y \text{ axes}, \\ \mathbf{v}|_{t=0} = \mathbf{v}_0. \end{cases} \tag{4.4}$$

The source term $\mathbf{f}$ is constant and given by

$$\mathbf{f} = \left(\frac{u_*^2}{H}, 0, 0 \right). \tag{4.5}$$

ii) The initial data. The initial data $\mathbf{v}_0$ is a random perturbation of the field

$$\mathbf{U}(x, y, z) = \left(\left(\frac{\widetilde{z}}{H} \right)^{\frac{1}{7}}, 0, 0 \right), \tag{4.6}$$

[8] numerically more convenient, theoretically equivalent to the standard Navier-Stokes equations

where $\widetilde{z} = \min(z, 2H - z)$. The corresponding profile coincides more or less with the log profile, without the singularity at $z = 0$ and $z = L_z$. In order to get a flow that is not too trivial and looks like a turbulent flow, we take $\mathbf{v}_0$ such that

$$\mathbf{v}_0 = \mathbf{U} + 0.125\eta(x, y, \widetilde{z}, \omega) \left(\left(\frac{\widetilde{z}}{H} \right)^{\frac{1}{7}}, 1, 1 \right). \tag{4.7}$$

The function $\eta \in [-1, 1]$ is a zero mean Gaussian random variable: at each point (x, y, z) and each run labeled by ω, the code randomly picks a number $\eta(x, y, z, \omega)$, thanks to a standard numerical random generator. This field is not divergence-free, but the code automatically correct this error at the first time step, through the incompressibility condition.

iii) Parameters of the simulations. They are the same as those of MOSER-KIM-MANSOUR [37], which is our benchmark. We have performed four DNS: three of them are in the flat case (see figure 2), for $Re_\star = 180, 360, 550$, and one in the rough case (see figure 1) for $Re_\star = 180$.
Let Δt denotes the time step, T the final time of the simulation, (n_x, n_y, n_y) determines the mesh size, which means that the discretization space-step Δa in the a-axis $(a = x, y, z)$ is given by

$$\Delta a = \frac{L_a}{n_a}.$$

Run	(L_x, L_y, L_z)	(n_x, n_y, n_z)	Δt	T
DNS-FLAT-180	$(4\pi, 4/3\pi, 2)$	$(128, 128, 128)$	0.005	$3600\nu/u_\star^2$
DNS-FLAT-360	$(2\pi, 2/3\pi, 2)$	$(256, 128, 192)$	0.0025	$3600\nu/u_\star^2$
DNS-FLAT-550	$(2\pi, 2/3\pi, 2)$	$(256, 256, 257)$	0.00125	$1800\nu/u_\star^2$
DNS-ROUGH -180	$(4\pi, 4/3\pi, 2)$	$(128, 128, 128)$	0.005	$3600\nu/u_\star^2$

Table 1: Parameters for each DNS

Since the Kolmogorov scale is getting smaller as $Re_\star$ increases, the computational cost is dramatically expensive for large $Re_\star$. This is why the dimensions of the computational boxes in DNS-FLAT-360 and 550 are smaller than the dimensions in DNS-FLAT-180.

iv) Results in the flat case.[9] Our results are reported in figure 3 where we have plotted the mean adimensionalized streamwise component of the velocity as well as the results of Moser et all MOSER-KIM-MANSOUR [37]. In particular, if $\mathbf{v}_{\text{DNS}} = (u_{\text{DNS}}, v_{\text{DNS}}, w_{\text{DNS}})$ denotes the calculated field by the DNS,

$$\overline{u}(z) = \frac{1}{T n_x n_y} \sum_{n=0}^{T/\Delta t} \sum_{j=0}^{n_x} \sum_{k=0}^{n_y} u_{\text{DNS}} \left(n\Delta t, j\frac{L_x}{n_x}, k\frac{L_y}{n_y}, z \right). \tag{4.8}$$

We observe a very good correspondence between our results of those of MOSER-KIM-MANSOUR [37], at least in average. This validates our DNS in the flat case, which allows us to think that our DNS in the rough case[10], outlined below, is accurate.

v) The rough case. The rough topography displayed in figure 1 is built in three steps as follows.

[9] For the simplicity, the overline always means an average which will be specified case by case, to avoid the risks of confusion. We also may use $\langle \cdot \rangle$ for time averages.

[10] So far we know, there is no available data in the literature for such a rough case.

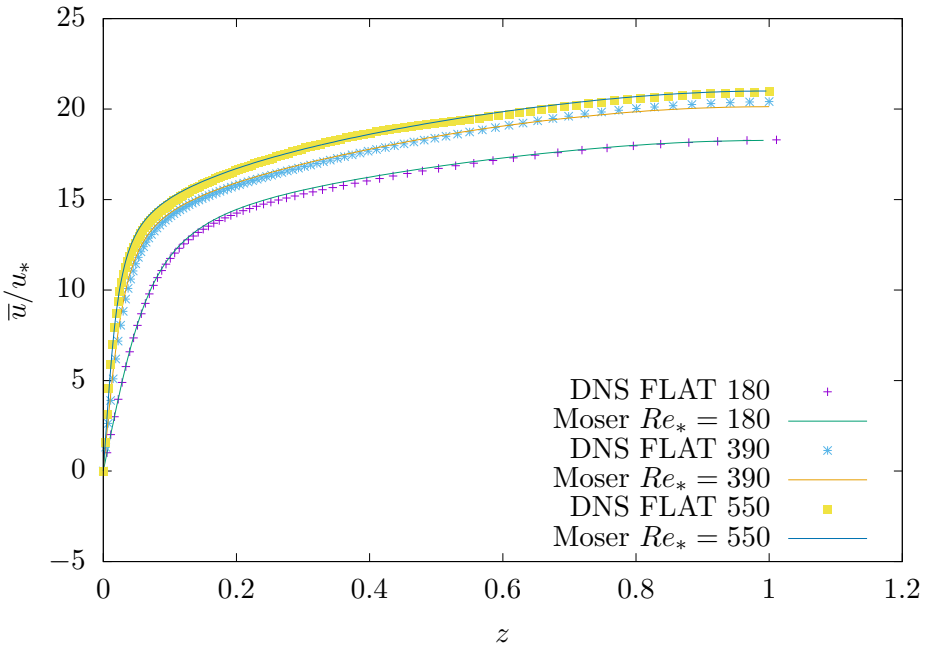

Figure 3: Streamwise velocity profile compared to those provided by Moser-Kim-Mansour [37].

1) We construct regularly spaced Gaussian domes centered at (x_i, y_i) with random heights $\tilde{\Lambda}_i$ and variances σ_i, leading to the primary topography $z = \tilde{\Lambda}(x, y)$ given by

$$\tilde{\Lambda}(x,y) = \sum_{i=1}^{N} \tilde{\Lambda}_i e^{-[(x-x_i)^2+(y-y_i)^2)]/(4\sigma_i^2)}. \tag{4.9}$$

2) This topography remains regular. In order to make it more chaotic, we follow the idea of Rossi [43] and we pick Gaussian domes Λ_j again, as well as random angles θ_j and aspect ratio a_j. Then we perturb $\tilde{\Lambda}(x, y)$ as follows:

$$\Lambda(x,y) = \tilde{\Lambda}(x,y) + \sum_{j=1}^{N} \Lambda_j e^{-[[c_j(x-x_j)+s_j(y-y_j)]^2/a_j^2+[c_j(y-y_j)-s_j(x-x_j)]^2 a_j^2]/(4\sigma_j^2))}, \tag{4.10}$$

where $c_j = \cos(\theta_j)$, $s_j = \sin(\theta_j)$, a_j. The Λ_j's, the θ_j'a and the a_j's are all Gaussian as well.

3) The roughness field is normalized such that $max(\Lambda(x, y)) = h_{max} = 0.1$. Therefore, the bottom is the surface given by: $z = \Lambda(x, y)$.

To perform the simulation, we use the "immersed boundary method" (IBM), initially developed by Peskin [41] (see also Lewandowski-Pichot [33]). This consists of solving the Navier-Stokes equation in $\Omega = [0, L_x] \times [0, L_y] \times [0, L_z]$, by adding in the Navier-Stokes equations (4.4) the additional source term

$$-\frac{1}{\varepsilon} \mathbb{1}_{\{0 \le z \le \Lambda(x,y)\}} \mathbf{v}, \tag{4.11}$$

for a small value of ε, which does not change the standard results and analysis about the Navier-Stokes equations[11]. This additional term enforces $\mathbf{v}$ to be negligible for $z \leq \Lambda(x, y)$, and does not affect the system in the domain $\Lambda(x, y) \leq z \leq L_z$. The results of the

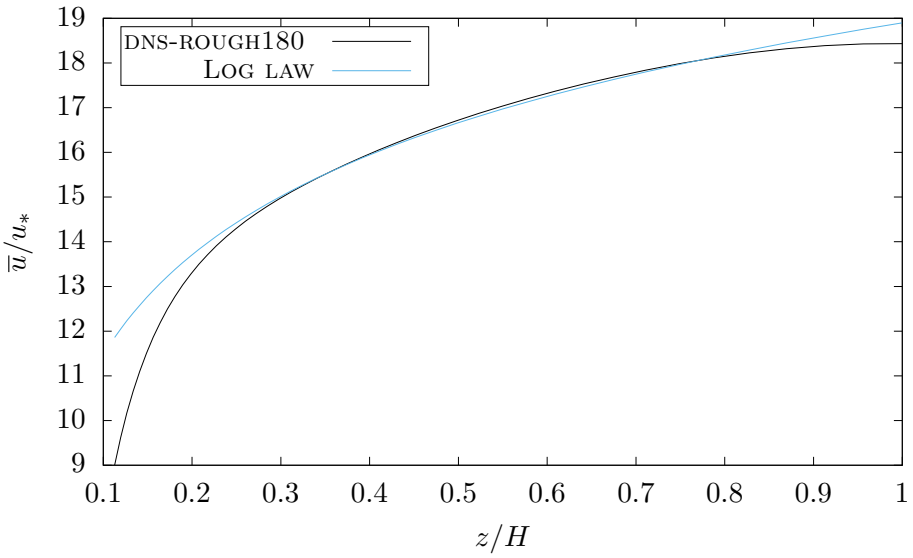

Figure 4: Streamwise velocity profile compared to a log profile.

simulation are reported in figure 4. We also have plotted on the same figure the log profile given by

$$h(z) = \frac{1}{0.31} \ln\left(\frac{z}{0.025}\right) + 7.0.$$

Our simulation yields a mean streamwise profile that perfectly matches with this log law for $z \in [0.3, 0.8]$, thereby validating our DNS.

4.2 Determination of the mixing length and the constants

The aim of this section is to derive from the DNS a formula to determine the mixing length ℓ. We also settle the values of the constants C_v and C_k involved in the boundary conditions at Γ_c for $\mathbf{v}$ and k.

4.2.1 General methodology

Let $\mathscr{E}$ denotes the total mean dissipation, given by

$$\mathscr{E} = 2\nu\overline{|\nabla \mathbf{v}|^2}. \tag{4.12}$$

It is common in turbulence modeling to assume that ℓ is a function of k and $\mathscr{E}$, that is $\ell = \ell(k, \mathscr{E})$. A straightforward dimensional analysis yields the formula

$$\ell = \frac{k\sqrt{|k|}}{\mathscr{E}}, \tag{4.13}$$

on which the determination of ℓ is based. We assume that ℓ does not depend on x and y. Therefore in this framework, the means are calculated from the data by the same formula

[11] The comprehensive mathematical analysis of the IBM is carried out in LEWANDOWSKI-PICHOT [33].

as (4.8). To be more specific, if Ψ is any field related to the flow, Ψ_{DNS} the corresponding calculated field, then

$$\overline{\Psi}(z) = \frac{1}{Tn_xn_y}\sum_{n=0}^{T/\Delta t}\sum_{j=0}^{n_x}\sum_{k=0}^{n_y}\Psi_{\text{DNS}}\left(n\Delta t, j\frac{L_x}{n_x}, k\frac{L_y}{n_y}, z\right). \tag{4.14}$$

Of course, only numerical values of $\overline{\Psi}$ at $z = qL_z/n_z$ $(q = 0, \cdots, n_z)$ can be calculated by (4.14). Based on this, our procedure is the following:

i) we compute $\overline{\mathbf{v}} = \overline{\mathbf{v}}(z)$ by (4.14),

ii) at each grid point, we form the field $\mathbf{v}'_{vert} = \mathbf{v}_{\text{DNS}} - \overline{\mathbf{v}}$,

iii) we extract from the data the numerical TKE denoted by k_{vert}, given at each $z = qL_z/n_z$ by the quantity $k_{vert}(z) = (1/2)\overline{|\mathbf{v}'_{vert}|^2}(z)$,

iv) by the standard finite difference scheme, we calculate $\mathscr{E}_{vert} = \mathscr{E}_{vert}(z)$ by (4.12),

v) we get at each $z = qL_z/n_z$ the mixing length $\ell = \ell(z)$ by forming the quotient $k_{vert}(z)\sqrt{k_{vert}(z)}/\mathscr{E}_{vert}(z)$.

Remark 4.1. *The function $k_{vert}(z)$ calculated above is the horizontal mean of the TKE. This is the appropriate quantity for the determination of ℓ, according to the horizontal homogeneity assumption. To calculate the full TKE from the DNS, we must use the time average over the simulation time:*

$$\langle\psi\rangle(\mathbf{x}) = \frac{1}{T}\sum_{n=0}^{T/\Delta T}\psi_{DNS}(n\Delta T, \mathbf{x}), \tag{4.15}$$

where $\mathbf{x} = (x, y, z)$. Then the Reynolds decomposition is written as $\mathbf{v}_{DNS} = \langle\mathbf{v}\rangle + \mathbf{v}'_{DNS}$, yielding

$$k_{DNS}(\mathbf{x}) = (1/2)\langle|\mathbf{v}'_{DNS}|^2\rangle. \tag{4.16}$$

We have plotted in figure 5 the curves of ℓ we have obtained by this way, in terms of the non dimensional variable $z' = z/H$.

4.2.2 Universal formula for the mixing length

We observe that the mixing length is increasing in the beginning of the turbulent layer (until $z \approx 0.6$) and slighly decreases until $z = 1$. Our goal is to interpolate these curves to get a universal formula in terms of the $Re_\star$ and z, by an empirical method.
Figure 5 suggests to seek for exponential profils. However, it is usually accepted that near $z = 0$, ℓ is of the form $\ell = \kappa z$. Therefore, we multiply this exponential profile by an hyperbolic tangent function, which is an approximation of the Heaviside function. Finally, since ℓ is non-zero within the viscous sublayer, we add a term that depends on the natural length scale $\nu/u_\star = H/Re_\star$. These considerations have led us to introduce the following empirical formula by trial and error:

$$\ell = K\tanh\left(A\left(Re_\star\frac{z}{H} - B\right)\right)\exp\left(-Re_\star^2\frac{\left(\frac{z}{H} - \frac{z_i}{H}\right)^2}{2\sigma}\right) + 75\frac{H}{Re_\star} \tag{4.17}$$

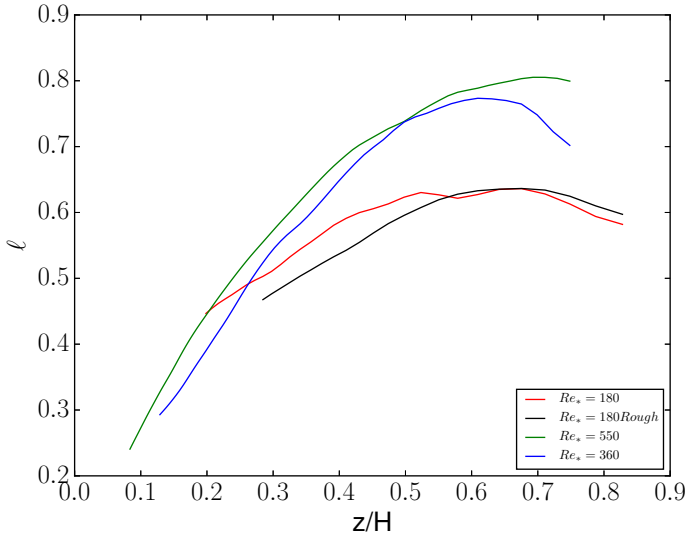

Figure 5: Profils of ℓ calculated from the DNS

where $z_i = 0.6H\,m$. In the rough case, by comparing the red line to the dark line in figure 5 (DNS-FLAT 180 and DNS-ROUGH 180) we apply a correction that takes the topography into account, which gives:

$$\ell = K \tanh\left(A\left(Re_\star \frac{z+z_R}{H} - B\right)\right) \exp\left(-Re_\star^2 \frac{\left(\frac{z+z_R}{H} - \frac{z_i}{H}\right)^2}{2\sigma}\right) + 75\frac{H}{Re_\star} \tag{4.18}$$

where $z_R = 0.05H\,m$ is the mean value of the roughness, estimated from Figure 5. It remains to settle the coefficients A, B, σ and K. They are sought to be function of $Re_\star$ only. As we shall show it in the following, we get the following laws for large values of $Re_\star$ (valid from $Re_\star = 900$, depending on the coefficients):

$$A = 3.05 Re_*^{0.065}, \tag{4.19}$$

$$B = 0, \tag{4.20}$$

$$\sigma = 0.3 Re_*^{1.05}, \tag{4.21}$$

$$K = 0.32 Re_*^{0.12}. \tag{4.22}$$

Moreover, it is accepted that near $z = 0$, $\ell = \kappa z$ where κ is the von Kármán constant. However, according to figure 7, although ℓ follows well a linear law near $z = 0$, its slope looks non constant when $Re_\star$ varies. Indeed, we obtain from our graphs (see Figure 12 below) the following law, valid from $Re_\star \approx 800$:

$$\kappa = \kappa(Re_\star) = 0.25(Re_\star)^{0.32} \quad \text{hence} \quad \ell = 0.25(Re_\star)^{0.32} z. \tag{4.23}$$

However, we observe in Figure 12 that the usual law is valid for instance when $Re_\star = 180$. The law (4.17) must be checked for high values of $Re_\star$, which is done by applying the algorithm to the results of Moser and al in Figure 7, and also yields the laws satisfied by the coefficients A, B, σ and K for high values of $Re_\star$, also used in the rough case.
In Figures 8 and 9, we have plotted the values of the constants A and B.
Figure 10 shows that the coefficient σ follows a linear law for all $Re_\star$, hence (4.19).

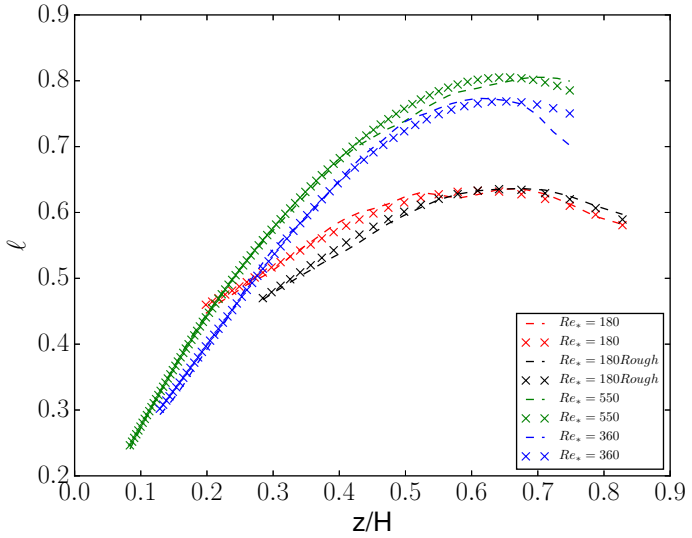

Figure 6: Dotted lines draw the mixing length calculated from the DNS, Crosses draw curves from formula (4.17) and (4.18)

4.2.3 Determination of the constants

We recall that the eddy viscosities/diffusion ν_t and μ_t are given by

$$\nu_t(k) = C_v \ell \sqrt{k}, \quad \mu_t(k) = C_k \ell \sqrt{k}.$$

Now that we know how to compute ℓ thanks to (4.17), we are able to estimate the constants C_v and C_k as follows. In this section, $\langle \psi \rangle$ denotes the time average over the time simulation defined by (4.15), and the TKE k in the formulae below is given by (4.16). Because of the horizontal homogeneity assumption, we focus on the vertical components of the Reynolds stress, linked to the eddy coefficients by:

$$\langle u'_{\mathrm{DNS}} w'_{\mathrm{DNS}} \rangle = \nu_t \frac{\partial \langle u_{\mathrm{DNS}} \rangle}{\partial z} = C_v \ell \sqrt{k_{\mathrm{DNS}}} \frac{\partial \langle u_{\mathrm{DNS}} \rangle}{\partial z}, \tag{4.24}$$

and

$$\langle e'_{\mathrm{DNS}} w'_{\mathrm{DNS}} \rangle = \mu_t \frac{\partial k_{\mathrm{DNS}}}{\partial z} = C_k \ell \sqrt{k_{\mathrm{DNS}}} \frac{\partial k_{\mathrm{DNS}}}{\partial z}. \tag{4.25}$$

Hence, C_v is the value that minimizes the error in (4.24) whereas C_k is the value that minimizes the error in (4.25). By the least square method, C_v is such that

$$\sum_{i=1}^{N} \left(\langle u'_{\mathrm{DNS}} w'_{\mathrm{DNS}} \rangle(\mathbf{x}_i) - C_v \ell(z_i) \sqrt{k_{\mathrm{DNS}}(\mathbf{x}_i)} \frac{\partial \langle u_{\mathrm{DNS}} \rangle}{\partial z}(\mathbf{x}_i) \right)^2 \tag{4.26}$$

is minimum, and C_k is such that

$$\sum_{i=1}^{N} \left(\langle e'_{\mathrm{DNS}} w'_{\mathrm{DNS}} \rangle(\mathbf{x}_i) - C_k \ell(z_i) \sqrt{k_{\mathrm{DNS}}(\mathbf{x}_i)} \frac{\partial k_{\mathrm{DNS}}}{\partial z}(\mathbf{x}_i) \right)^2 \tag{4.27}$$

is minimum, where $\{\mathbf{x}_1, \cdots, \mathbf{x}_N\}$ denotes the grid points set, $\mathbf{x}_i = (x_i, y_i, z_i)$. This optimization problem has been solved by the *brute-force* method [3], based on the results of DNS-FLAT 180, DNS-FLAT 550 and the corresponding profiles for ℓ. We get:

$$C_k = 0.15 \quad C_v = 0.105 \tag{4.28}$$

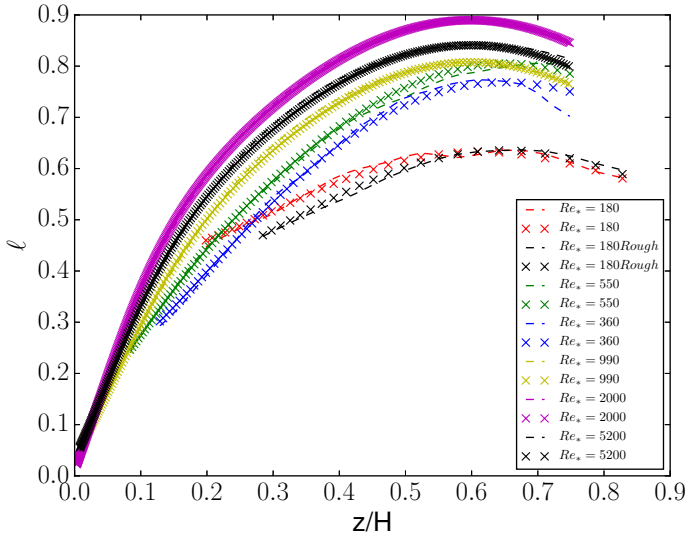

Figure 7: Lines are results from Moser and al [37], Crosses results from formulae (4.17) and (4.18)

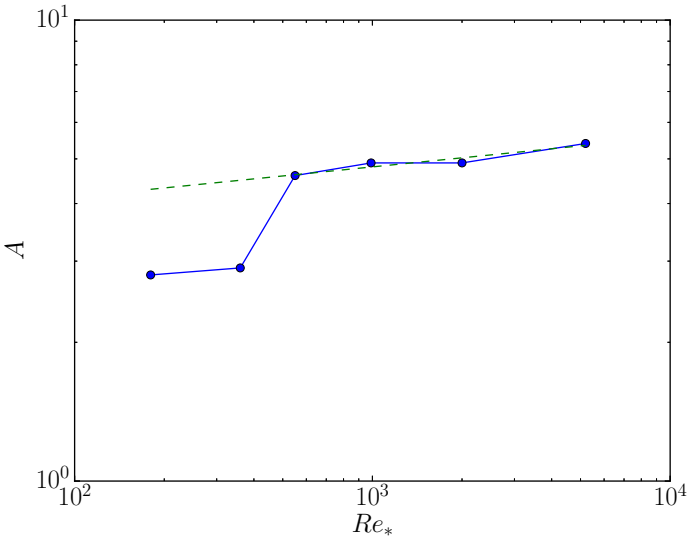

Figure 8: $A = A(Re_\star)$. The green dotted line is the 0.065 slope.

Remark 4.2. *We find in [35, Chapter 4]: $C_v = C_k = 0.09$. However, these values have been calibrated for the full $k - \mathscr{E}$ model, which can explain the slight difference with our results.*

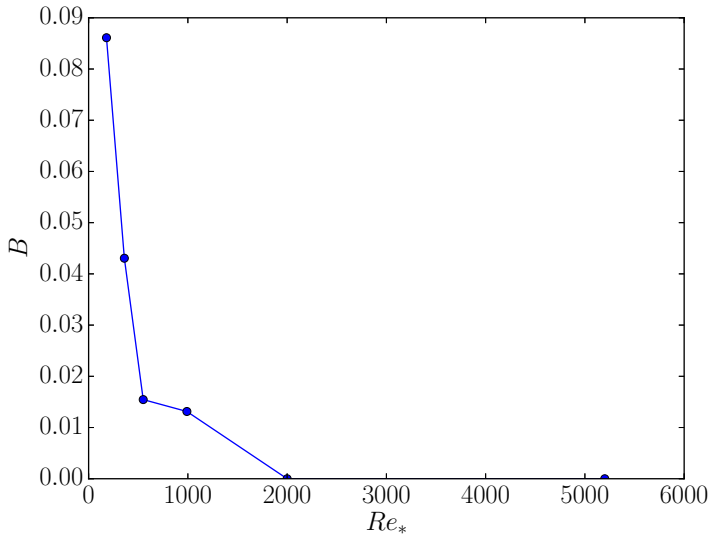

Figure 9: $B = B(Re_\star)$

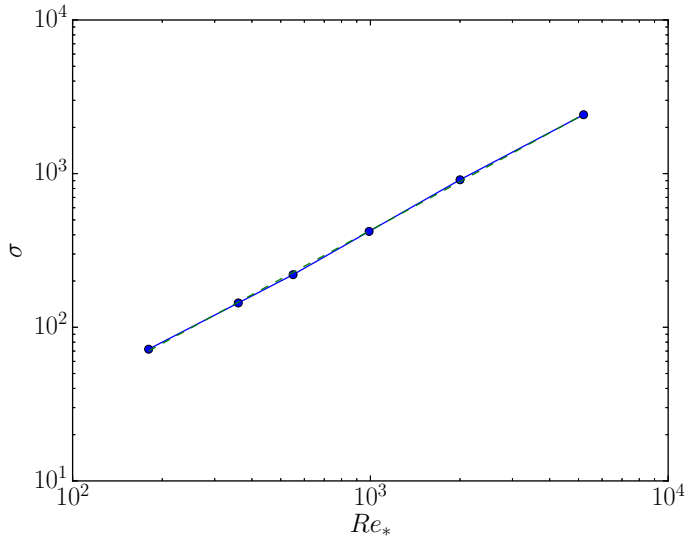

Figure 10: $\sigma = \sigma(Re_\star)$. The green doted line is the 1.05 slope.

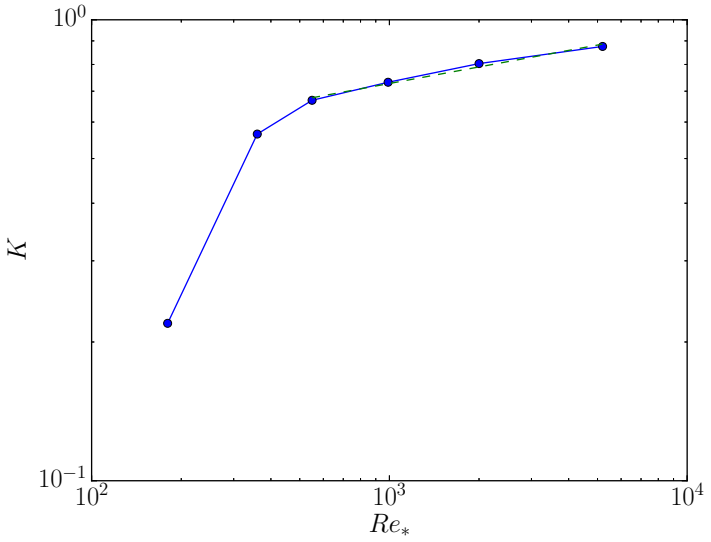

Figure 11: $K = K(Re_\star)$. The green dotted line is the 0.12 slope.

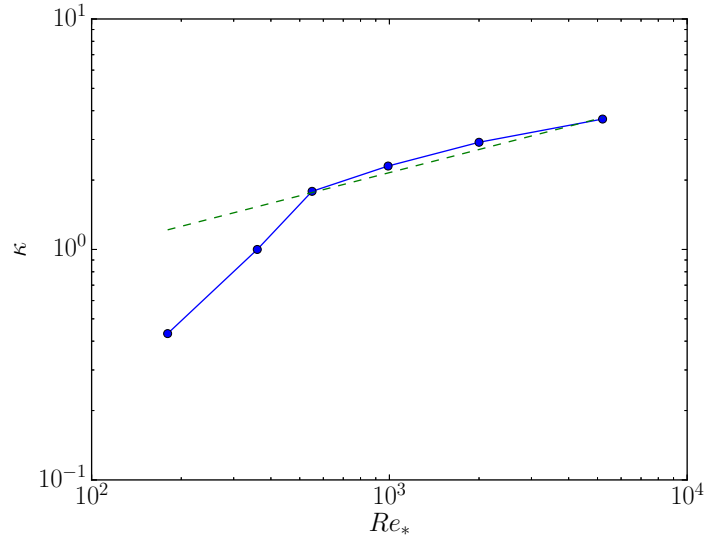

Figure 12: $\kappa = \kappa(Re_\star)$. The green dotted line is the 0.32 slope.

5 NSTKE simulations and conclusions

5.1 Algorithm and settings

Our code is based on the SIMPLEC algorithm (Patankar [39], Issa [23]), that we have adapted to the NSTKE equations, leading to encode the following iterations. At step n, $(\mathbf{v}^{n-1}, p^{n-1}, k^{n-1})$ being known, we first solve the velocity equation

(5.1)
$$\left\{\begin{array}{rcll} (\overline{\mathbf{v}}^{n-1}\cdot\nabla)\,\overline{\mathbf{v}}^{n} - \nabla\cdot\left[(2\nu+\nu_t(k^{n-1}))\,D\overline{\mathbf{v}}^{n}\right] + \nabla p^{n-1} &=& \mathbf{f} & \text{in } \mathrm{Om}_c,\\ \nabla\cdot\overline{\mathbf{v}}^{n} &=& 0 & \text{in } \mathrm{Om}_c,\\ -[(2\nu+\nu_t(k^{n-1}))D\overline{\mathbf{v}}^{n}\cdot\mathbf{n}]_\tau &=& \alpha_v|\overline{\mathbf{v}}^{n-1}|\overline{\mathbf{v}}^{n} & \text{on } G_c,\\ \overline{\mathbf{v}}^{n}\cdot\mathbf{n} &=& 0 & \text{on } G_c, \end{array}\right.$$

which is a standard elliptic equation, with the added difficulties presented by the incompressibility constraint and the boundary condition $\overline{\mathbf{v}}^{n}\cdot\mathbf{n}|_{G_c}=0$. Once $\mathbf{v}^n$ is calculated, we solve the TKE equation:

(5.2)
$$\left\{\begin{array}{rcll} \overline{\mathbf{v}}^{n}\cdot\nabla k^{n} - \nabla\cdot[(\mu+\mu_t(k^{n-1})\nabla k^{n}] &=& \nu_t(k^{n-1})|D\overline{\mathbf{v}}^{n}|^2 - \dfrac{k^n\sqrt{|k|^{n-1}}}{\ell} & \text{in } \mathrm{Om}_c,\\ -(\mu+\mu_t(k^{n-1}))\dfrac{\partial k^n}{\partial\mathbf{n}} &=& \alpha_k k^n\sqrt{|k|^{n-1}} & \text{on } G_c. \end{array}\right.$$

Finally, the pressure is calculated by the Poisson equation:

(5.3)
$$\left\{\begin{array}{rcll} \Delta p^n &=& -\nabla\cdot\left(\nabla\cdot(\mathbf{v}^n\otimes\mathbf{v}^{n-1}) - \nabla\cdot\left[(2\nu+\nu_t(k^{n-1}))\,D\mathbf{v}^n\right] - \mathbf{f}\right) & \text{in } \mathrm{Om}_c,\\ \dfrac{\partial p^n}{\partial\mathbf{n}} &=& 0 & \text{on } G_c. \end{array}\right.$$

System (5.1)-(5.2)-(5.3) for a given n, satisfies periodic boundary conditions in the $x-y$ axes. The source term $\mathbf{f}$ is given by (4.5). We implement this scheme in the OpenFoam solver (see at `https://www.openfoam.com`), based on the second order finite volumes method (see in Eymard-Gallouet-Herbin [19]).

Remark 5.1. *Although we observe a good numerical convergence (see section 5.2.3 below), we have no mathematical proof of the convergence of this scheme to the NSTKE model, which is a difficult open question. Usually, we know that such scheme does converge when the eddy viscosity is close to a constant and when the source term is small enough in some sense (see in Lewandowski [32]). However, it is likely that the homogeneous Neumann boundary condition for the pressure in the equation (5.3) may yield serious complications in a mathematical convergence analysis.*

We have carried out four simulations in the flat case for high Reynolds numbers, namely $Re_\star = 990, 2000, 5200, 10000$. Then we have tested the rough case for $Re_\star = 5200, 10000$. The mixing length is given by (4.17) (flat case) and (4.18) (rough case), the constants C_v and C_k by (4.28). The iterations (5.1)-(5.2)-(5.3) are initialized by

$$\mathbf{v}^0 = (u^0, 0, 0), \quad u^0 = 1\,ms^{-1}; \quad k^0 = 10^{-3}\,m^2s^{-2}; \quad p^0 = 0\,Pa. \tag{5.4}$$

The parameter settings are given in Table 2. The coefficients α_v and α_k have been determined up to $Re_\star = 5000$ by solving the minimization problem

$$\min\{||\mathbf{v}_{\mathrm{NSTKE}} - \mathbf{v}_{\mathrm{DNS}}||_2^2 + ||k_{\mathrm{NSTKE}} - k_{\mathrm{DNS}}||_2^2\}. \tag{5.5}$$

Run	(L_x, L_y, L_z)	(n_x, n_y, n_z)	α_v	α_k
NSTKE-FLAT-990	$(6.28, 4.18, 2)$	$(16, 16, 32)$	0.000125	0.04
NSTKE-FLAT-2000	$(6.28, 4.18, 2)$	$(16, 16, 32)$	0.0000525	0.01
NSTKE-FLAT-5200	$(6.28, 4.18, 2)$	$(16, 16, 32)$	0.000035	0.0005
NSTKE-FLAT-10000	$(6.28, 4.18, 2)$	$(16, 16, 64)$	0.000035	0.0005
NSTKE-ROUGH-5200	$(6.28, 4.18, 2)$	$(32, 24, 64)$	0.000035	0.0005
NSTKE-ROUGH-10000	$(6.28, 4.18, 2)$	$(32, 24, 64)$	0.00035	0.0005

Table 2: Parameters settings

The resolution of problem (5.5) is based on a standard dichotomy algorithm (see for instance in Teghem [50]). We have kept the same values for $Re_\star = 10000$, in the flat case as well as in the rough case, in the absence of DNS. Notice that the mesh sizes in this case are much more coarser than those used for the DNS, which is an undeniable advantage of the model. However, considering that the height of the viscous sublayer is negligible compared to this resolution, we have taken $z_0 = 0$ in the simulations for the flat case. The number of iterations is of order 1000.

5.2 Numerical Results in the flat case

5.2.1 Streamwise velocity

The results we get are compared to those of the high Reynolds numbers DNS provided in Lee-Moser [27], up to $Re_\star = 5200$. Experiments of turbulent channel flow at the high friction velocity based Reynolds number of 10000 does not currently exist in literature, to the extent of the authors knowledge. The existence of the logarithmic profile for channel flow at a friction velocity based Reynolds of 8000 for which data has been published from Yamamoto-Tsuji [52]. As a consequence, the velocity profile is compared to the logarithmic profile such as the studies of neutral atmospheric boundary layer Chow-Street-Xue-Ferziger [16].

The NSTKE model yields a departure from the log law. However, things seem better

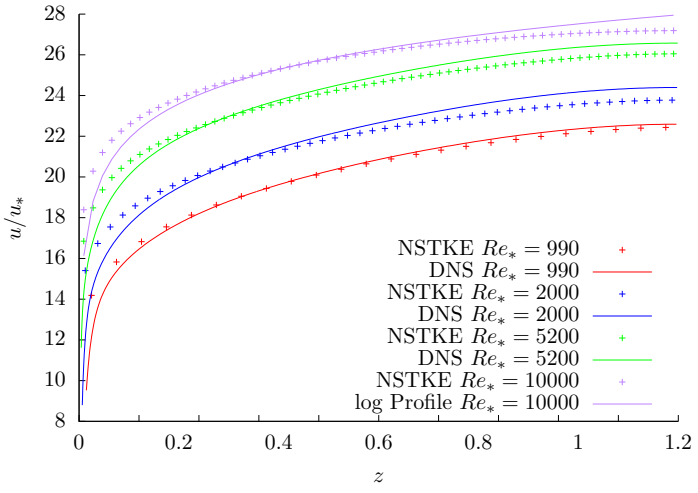

Figure 13: NSTKE Flat case. Non dimensional streamwise velocity

when $Re_\star$ increases, which may be only a trend reversal near the bottom. To corroborate

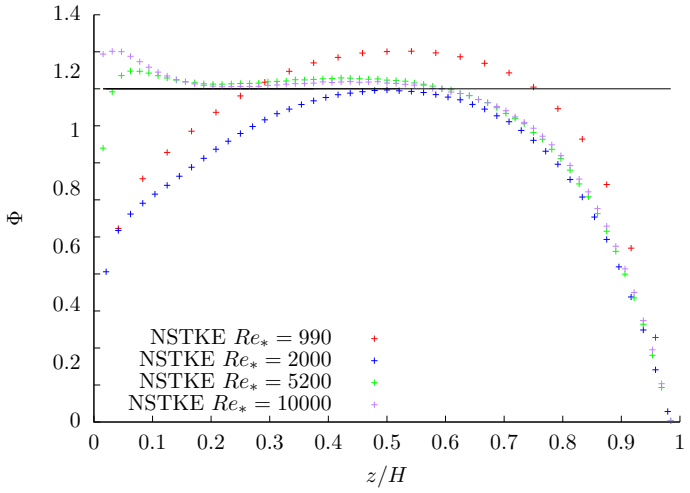

Figure 14: NSTKE Flat case. Comparison of the non dimensional mean shear Φ computed by the NSTKE model for the High Reynolds number simulations.

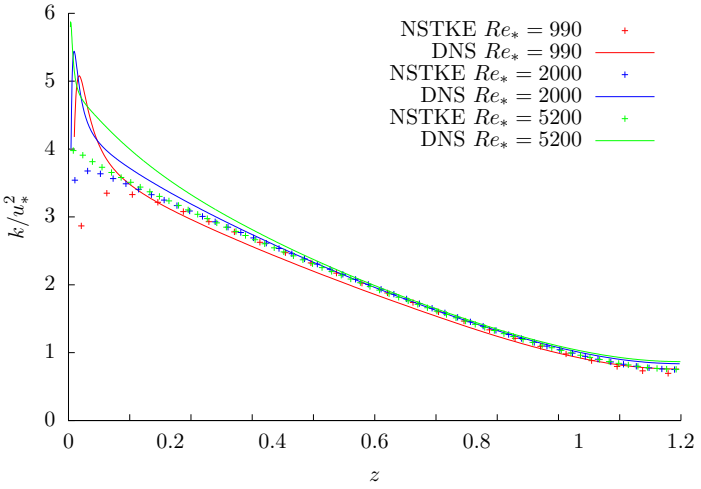

Figure 15: NSTKE Flat case. Turbulent kinetic energy

these observations, we have calculated the non dimensional mean shear defined by

$$\Phi = \frac{\kappa z}{u_*} \frac{\partial \overline{u}}{\partial z}, \tag{5.6}$$

which is equal to 1 when the profile is logarithmic. The results are plotted in Figure 14. The streamwise velocity given by the NSTKE model has a serious lack of shear at the top and the bottom of the boundary layer.

5.2.2 Turbulent kinetic energy

The turbulent kinetic energy is plotted on Figure 15, compared with the DNS results.The model overestimates the TKE at the bottom of the boundary layer.

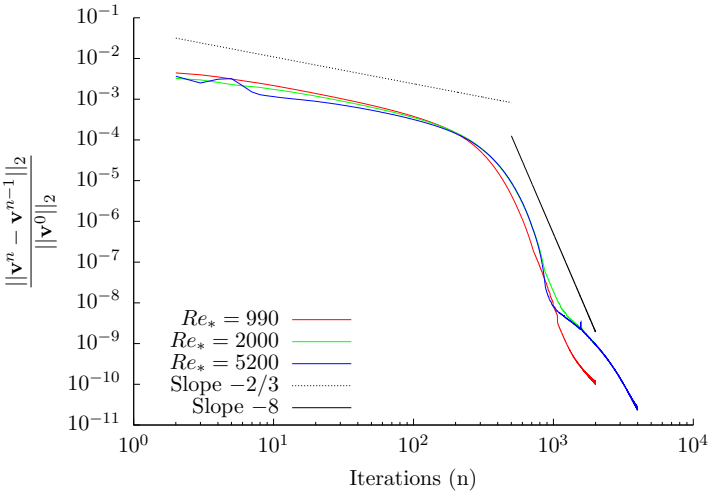

Figure 16: Convergence analysis.

5.2.3 Convergergence analysis

The convergence of the SIMPLEC algorithm for the NSTKE problem is shown in figure 16 for the $Re_\star = 900, 2000, 5200$ cases. The black lines indicates the slope of the decreasing rate, which is proportional to $n^{-2/3}$ for the first 300 iterations and increases up to n^{-8} until $n = 1000$, which is a good convergence result.

5.2.4 Corrected mixing length

The previous sections show that the NSTKE model does not perfectly reproduce the standard boundary layer profiles. It may come from the mixing length formula (4.17) and the law (4.19) that determines the main coefficient in the formula for ℓ, denoted by A. To fix this issue, we have replaced A by another coefficient of the form λA, the best choice of λ being equal to 0.608, after some simulations. As shown by the figure (17), the corrected model accurately reproduces the log profile up to $z = 0.7H$, which is quite satisfactory. About the TKE, it does not change much, in particular at high Reynolds number.

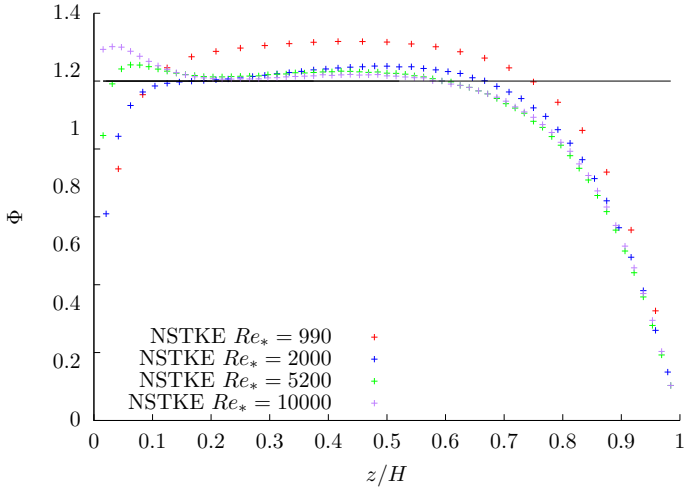

Figure 17: NSTKE Flat case. Mean shear Φ with the corrected mixing length profile.

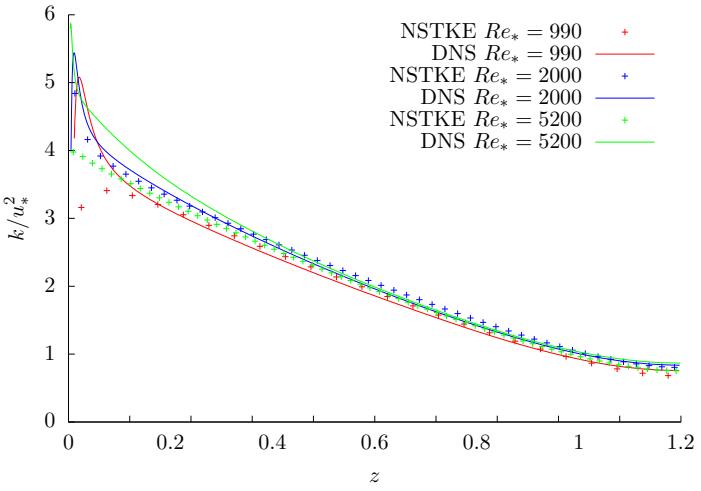

Figure 18: NSTKE Flat case. Turbulent kinetic energy with the corrected mixing length profile.

5.3 Numerical results in the rough case

The simulation is carried out from $z_0 = 0.1$. This is as if we have put a flat plate over the domes, starting the simulation from z_0 as in the flat case, the information about the topography being contained in the formula for ℓ, the boundary condition and the corresponding coefficients. We have applied the same correction for the coefficient A in formula (4.18) as in the flat case (see section 5.2.4 above). The results are reported in Figure 19, Figure 20 and Figure 21, following the same order as in the flat case. Without any DNS, the only way to analyse the results is the comparison with log profiles. We observe a departure from the log law outside the interval $[0.5, 0.7]$. Considering the TKE profiles, the intensity of the turbulence for $Re_\star = 5000$ and $Re_\star = 5000$ looks to be different only from $z/H = 0.5$.

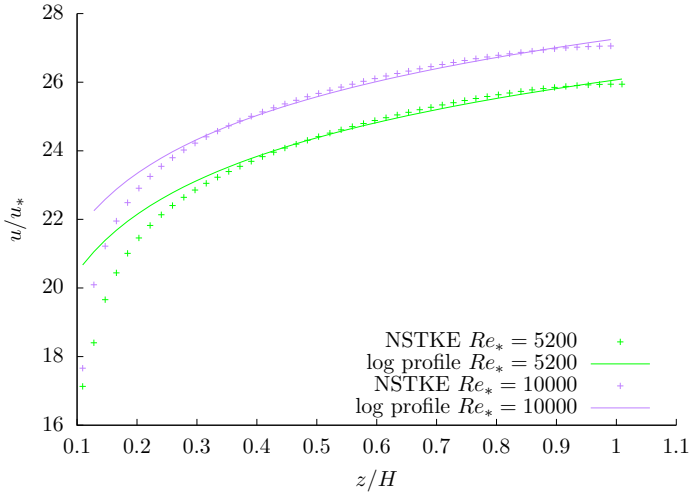

Figure 19: NSTKE Rough case. Non dimensional streamwise velocity.

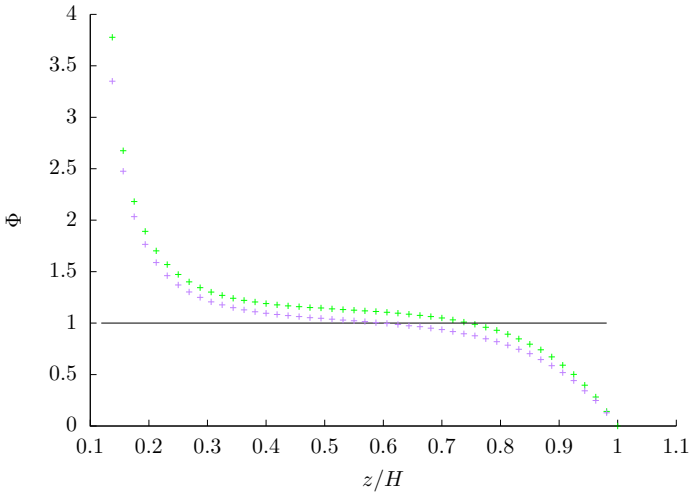

Figure 20: NSTKE Rough case. Mean shear

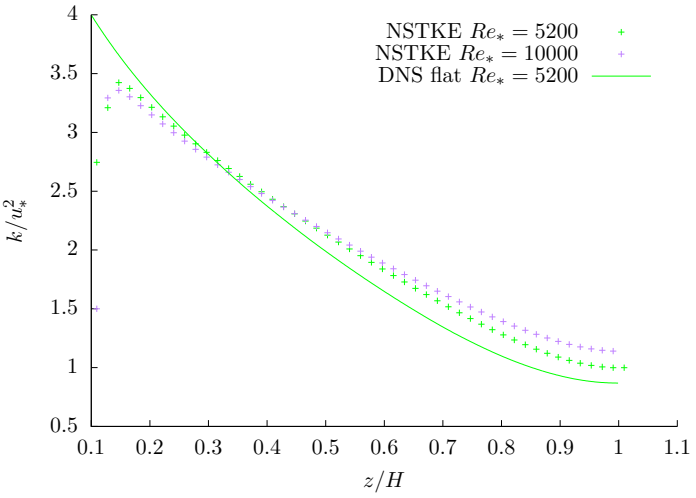

Figure 21: NSTKE Rough case. Turbulent kinetic energy

5.4 Some conclusions and perspectives

The NSTKE model yields satisfactory results in the flat case, although we had to adjust the formula calculated from the DNS for ℓ. The treatment of the pressure in the SIMPLEC algorithm could be questionable, in particular because of the boundary condition (5.3). Further simulation are probably necessary with another treatment of the pressure, following what was done in Chacon-Lewandowski [15, Chapters 13], where similar simulations for low Reynolds numbers are performed by the variational multi-scale method and a perturbation of the incompressibility constrain to resolve the pressure.
In the rough case, the present study cannot be considered as fully conclusive, but as a first step towards a general methodology to tackle this class of difficult numerical problems. These simulations suggest that the topography must be taken into account for the determination of the coefficients α_v et α_k in the boundary conditions (1.3) and (2.13), which has not been done already. The question is how to do that? Moreover, it is likely that ℓ does not depend on z only, but also on x, y in a way that depends on the topography. To fix this, several other DNS are necessary in the rough case, for the highest possible $Re_\star$,

expecting for a generic formula for $\ell(x, y, z, Re_\star)$, as well as $\alpha_a(x, y, z, Re_\star)$ $(a = v, k)$. This will be the subject of a next study.

References

[1] R.A. Adams and J. F. Fournier. Sobolev spaces, volume 140 of Pure and Applied Mathematics (Amsterdam). Elsevier/Academic Press, Amsterdam, second edition, 2003.

[2] C.D. Argyropoulos and N.C. Markatos. Recent advances on the numerical modelling of turbulent flows. Applied Mathematical Modelling, 39(2):693–732, 2015.

[3] R.A. Baeza-Yates. Algorithms for string searching. In AcM sIGIR Forum, volume 23, pages 34–58. ACM, 1989.

[4] B. Baldwin and T. Barth. A one-equation turbulence transport model for high reynolds number wall-bounded flows. In 29th Aerospace Sciences Meeting, page 610, 1991.

[5] B. Baldwin and H. Lomax. Thin-layer approximation and algebraic model for separated turbulentflows. In 16th aerospace sciences meeting, page 257, 1978.

[6] A.C. Bennis, T. Chacón-Rebollo, M. Gómez-Mármol, and R. Lewandowski. Numerical modelling of algebraic closure models of oceanic turbulent mixing layers. M2AN Math. Model. Numer. Anal., 44(6):1255–1277, 2010.

[7] L. Berselli and R. Lewandowski. On the reynolds time-averaged equations and the long-time behavior of leray-hopf weak solutions, with applications to ensemble averages. Nonlinearity, 32(11):4579–4608, 2019.

[8] B. Blanke and P. Delecluse. Variability of the tropical atlantic ocean simulated by a general circulation model with two different mixed-layer physics. J. Phys. Oceanogr., 23:1363–1388, 1993.

[9] L. Boccardo, J. I. Diaz, D. Giachetti, and F. Murat. Existence of a solution for a weaker form of a nonlinear elliptic equation. In Recent advances in nonlinear elliptic and parabolic problems (Nancy, 1988), volume 208 of Pitman Res. Notes Math. Ser., pages 229–246. Longman Sci. Tech., Harlow, 1989.

[10] L. Boccardo and T. Gallouët. Nonlinear elliptic and parabolic equations involving measure data. J. Funct. Anal., 87(1):149–169, 1989.

[11] L. Boccardo and F. Murat. A property of nonlinear elliptic equations when the right-hand side is a measure. Potential Anal., 3(3):257–263, 1994.

[12] H. Brezis. Functional analysis, Sobolev spaces and partial differential equations. Universitext. Springer, New York, 2011.

[13] M. Bulíček, R. Lewandowski, and J. Málek. On evolutionary Navier-Stokes-Fourier type systems in three spatial dimensions. Comment. Math. Univ. Carolin., 52(1):89–114, 2011.

[14] M. Bulíček, J. Málek, and K. R. Rajagopal. Navier's slip and evolutionary Navier-Stokes-like systems with pressure and shear-rate dependent viscosity. Indiana Univ. Math. J., 56(1):51–85, 2007.

[15] T. Chacòn-Rebollo and R. Lewandowski. Mathematical and Numerical Foundations of Turbulence Models and Applications. Modeling and Simulation in Science, Engineering and Technology. Springer New York, 2014.

[16] F.K. Chow, R.L. Street, M. Xue, and J.H. Ferziger. Explicit filtering and reconstruction turbulence modeling for large-eddy simulation of neutral boundary layer flow. Journal of the atmospheric sciences, 62(7):2058–2077, 2005.

[17] M. Cindori, F. Juretić, H. Kozmar, and I. Džijan. Steady rans model of the homogeneous atmospheric boundary layer. Journal of Wind Engineering and Industrial Aerodynamics, 173:289–301, 2018.

[18] J. Deleersnijder and P. Luyten. On the practical advantages of the quasi-equilibrium version of the mellor and yamada level 2.5 turbulence closure applied to marine modelling. Applied Mathematical Modelling, 18:281–287, 1994.

[19] R. Eymard, T. Gallouët, and R. Herbin. Finite volume methods. In Handbook of numerical analysis, Vol. VII, Handb. Numer. Anal., VII, pages 713–1020. North-Holland, Amsterdam, 2000.

[20] E. Fares and W. Schröder. A general one-equation turbulence model for free shear and wall-bounded flows. Flow, turbulence and combustion, 73(3-4):187–215, 2005.

[21] T. Foken. 50 years of the monin-obukhov similarity theory. Boundary-Layer Meteorology, 119:431–447, 2006.

[22] U. Frisch. Turbulence. Cambridge University Press, Cambridge, 1995. The legacy of A. N. Kolmogorov.

[23] R.I Issa. Solution of the implicitly discretised fluid flow equations by operator-splitting. Journal of Computational Physics, 62(1):40 – 65, 1986.

[24] G. Kalitzin, G. Medic, G. Iaccarino, and P. Durbin. Near-wall behavior of rans turbulence models and implications for wall functions. Journal of Computational Physics, 204(1):265–291, 2005.

[25] S. Laizet and E. Lamballais. High-order compact schemes for incompressible flows: A simple and efficient method with quasi-spectral accuracy. Journal of Computational Physics, 228(16):5989–6015, 2009.

[26] S. Laizet and N. Li. Incompact3d: A powerful tool to tackle turbulence problems with up to O(105) computational cores. International Journal for Numerical Methods in Fluids, 67:1735–1757, December 2011.

[27] M. Lee and R. D. Moser. Direct numerical simulation of turbulent channel flow up to $re_\tau = 5200$. Journal of Fluid Mechanics, 774:395–415, 2015.

[28] S. Lele. Compact finite difference schemes with spectral-like resolution. Journal of Computational Physics, 103(1):16 – 42, 1992.

[29] R. Lewandowski. Analyse mathématique et océanographie, volume 39 of Recherches en Mathématiques Appliquées [Research in Applied Mathematics]. Masson, Paris, 1997.

[30] R. Lewandowski. The mathematical analysis of the coupling of a turbulent kinetic energy equation to the Navier-Stokes equation with an eddy viscosity. Nonlinear Anal., 28(2):393–417, 1997.

[31] R. Lewandowski. Long-time turbulence model deduced from the Navier-Stokes equations. Chin. Ann. Math. Ser. B, 36(5):883–894, 2015.

[32] R. Lewandowski. On a one dimensional turbulent boundary layer model. To appear in PAFA on Analysis and PDE, https://hal.archives-ouvertes.fr/hal-02134034, 2020.

[33] R. Lewandowski and G. Pichot. Numerical simulation of water flow around a rigid fishing net. Comput. Methods Appl. Mech. Engrg., 196(45-48):4737–4754, 2007.

[34] F. Liu. A thorough description of how wall functions are implemented in openfoam. Proceedings of CFD with OpenSource Software, pages 1–33, 2016.

[35] B. Mohammadi and O. Pironneau. Analysis of the k-epsilon turbulence model. RAM: Research in Applied Mathematics. Masson, Paris; John Wiley & Sons, Ltd., Chichester, 1994.

[36] A. S. Monin and A. M. Obukhov. Basic laws of turbulent mixing in the surface layer of the atmosphere. Tr. Akad. Nauk. SSSR Geophiz. Inst., 24(151):163–187, 1954.

[37] R.-D. Moser, J. Kim, and N. Mansour. Direct numerical simulation of turbulent channel flow up to Re=590. Physics of Fluids, 11(4):943–945, 1999.

[38] A. Parente, C. Gorlé, J. Van Beeck, and C. Benocci. Improved k–ε model and wall function formulation for the rans simulation of abl flows. Journal of wind engineering and industrial aerodynamics, 99(4):267–278, 2011.

[39] S. Patankar. Numerical Heat Transfer and Fluid Flow. Series in computational methods in mechanics and thermal sciences. Taylor & Francis, 1980.

[40] C. Pelletier. Étude mathématique du problème de couplage océan-atmosphère incluent les échelles turbulentes. PhD thesis, Communauté Université Grenoble Alpes, 2018.

[41] C. Peskin. The immersed boundary method. Acta Numerica, 11:479–517, 2002.

[42] S.-B. Pope. Turbulent flows. Cambridge University Press, Cambridge, 2000.

[43] L.F. Rossi. High order vortex methods with deforming elliptical gaussian blobs 1: Derivation and validation. Technical report, Department of Mathematical Sciences, 2001.

[44] P. Sagaut. Large eddy simulation for incompressible flows. Scientific Computation. Springer-Verlag, Berlin, third edition, 2006. An introduction, Translated from the 1998 French original, With forewords by Marcel Lesieur and Massimo Germano, With a foreword by Charles Meneveau.

[45] H. Schlichting and K. Gersten. Boundary-layer theory. Springer-Verlag, Berlin, enlarged edition, 2000. With contributions by Egon Krause and Herbert Oertel, Jr., Translated from the ninth German edition by Katherine Mayes.

[46] AM Smith and Tuncer Cebeci. Numerical solution of the turbulent-boundary-layer equations. Technical report, DOUGLAS AIRCRAFT CO LONG BEACH CA AIRCRAFT DIV, 1967.

[47] P. Spalart and S. Allmaras. A one-equation turbulence model for aerodynamic flows. In 30th aerospace sciences meeting and exhibit, page 439, 1992.

[48] D.B. Spalding. A single formula for the law of the wall. Transactions of the ASME, Series E: Journal of Applied Mechanics, 28:339–391, 1966.

[49] Guido Stampacchia. Èquations elliptiques du second ordre à coefficients discontinus. Séminaire de Mathématiques Supérieures, No. 16 (Été, 1965). Les Presses de l'Université de Montréal, Montreal, Que., 1966.

[50] J. Teghem. Recherche opérationnelle Tome1. Ellipses, Paris, 2012.

[51] D.C. Wilcox. Turbulence modeling for CFD, volume 2. DCW industries La Canada, CA, 1998.

[52] Y. Yamamoto and Y. Tsuji. Numerical evidence of logarithmic regions in channel flow at $re_\tau = 8000$. Physical Review Fluids, 3(1):012602, 2018.